

Holographic Phase Retrieval and Reference Design

David A. Barmherzig* Ju Sun† Po-Nan Li‡ T.J. Lane§ Emmanuel J. Candès¶

April 23, 2019

Abstract

A general mathematical framework and recovery algorithm is presented for the holographic phase retrieval problem. In this problem, which arises in holographic coherent diffraction imaging, a “reference” portion of the signal to be recovered via phase retrieval is a priori known from experimental design. A generic formula is also derived for the expected recovery error when the measurement data is corrupted by Poisson shot noise. This facilitates an optimization perspective towards reference design and analysis. We employ this optimization perspective towards quantifying the performance of various reference choices.

1 Introduction

1.1 Phase Retrieval and Coherent Diffraction Imaging

The phase retrieval problem concerns recovering a signal from the squared magnitude of its Fourier transform. The problem can be stated symbolically as

$$\begin{aligned} \text{Given } & |\hat{X}(\omega)|^2 \doteq \left| \int_{t \in T} X(t) e^{-i\omega t} \right|^2 \quad \text{for } \omega \in \Omega, \\ \text{Recover } & X \end{aligned} \tag{1.1}$$

where T and Ω are the (possibly multidimensional) domains of the signal and its Fourier transform, respectively. Phase retrieval arises ubiquitously in scientific imaging, where one seeks to “image” or determine the structure of an object from various phaseless data measurements. Such settings include crystallography [Mil90], diffraction imaging [BDP⁺07], optics [Wal63], and astronomy [DF87].

Phase retrieval has gained enormous attention over the last two decades, largely due to an emerging imaging technique known as Coherent Diffraction Imaging, or CDI [MCKS99] (illustrated in Fig. 1). In CDI, a coherent beam source, often being an X-ray, is illuminated upon a sample of interest. Upon the beam reaching the sample, diffraction occurs and secondary electromagnetic waves are emitted which travel until reaching a far-field detector. The detector measures the photon flux and hence records the resulting diffraction pattern, which is approximately proportional to the squared magnitude of the Fourier transform of the electric field of the sample. One can, in principle, recover the structure of the sample from the diffraction pattern by solving the phase retrieval problem [Goo17, Jag16, SEC⁺15]. With the advent of extremely powerful X-ray light sources, such as X-ray Free-Electron Lasers (XFELs) [CBB⁺06] and synchrotron radiation [RVW⁺01], CDI is pushing the frontier of high-resolution imaging of biological and material specimens at the nanoscale [LZGJ⁺18, XMR⁺14, LHM⁺12, MIRM15].

*Institute for Computational and Mathematical Engineering, Stanford University, Stanford, CA 94305, U.S.A.

†Department of Mathematics, Stanford University, Stanford, CA 94305, U.S.A.

‡Department of Electrical Engineering, Stanford University, Stanford, CA 94305, U.S.A.

§SLAC National Accelerator Laboratory, Menlo Park, CA 94025, U.S.A.

¶Department of Mathematics and Department of Statistics, Stanford University, Stanford, CA 94305, U.S.A.



Figure 1: CDI setup. Image courtesy of [CLS15b].

1.2 Phase Retrieval Algorithms

The phase retrieval problem does not admit a unique solution, as the forward mapping in Eq. (1.1) maps signals related by certain intrinsic symmetries to the same set of measurements (these are discussed in detail in Section 2.1). Also, modulo these unavoidable ambiguities, there still may not be a unique solution. This nonuniqueness occurs frequently for one-dimensional signals, but only on a set of (Lebesgue) measure zero for two- or higher-dimensional signals [Hay82, SEC⁺15, BBE17, SC91]. Thus, for CDI experiments (which concern two- or three-dimensional signals), there is almost surely a unique solution up to the intrinsic ambiguities. Nevertheless, solving the problem is equivalent to solving a quadratic system—which is well known to be NP-hard [BTN01].

In practice, the phase retrieval problem is often cast as a nonconvex optimization problem, for which various alternating-projection type algorithms are commonly employed. The most notable one is Fienup’s Hybrid Input-Output (HIO) algorithm [Fie78]. Other practical variants include Relaxed Averaged Alternating Reflections (RAAR) [Luk05], Difference Map [ERT07], and Alternating Direction Method of Multipliers (ADMM) [WYLM12, BPC⁺11, BS17]. While often successful, these algorithms are not guaranteed to find the correct solution. They are also known to suffer from various problems such as stagnation at erroneous solutions, slow runtime, sensitivity to noise and parameter tuning [Mar07, Els03].

To mitigate these difficulties, a line of recent work has proposed to modify the typical CDI setup. This involves sequentially modulating either the beam pattern or the Fourier transform via random or deterministic masks, thereby gathering multiple-shot measurements [LCL⁺08, JJB⁺08, CLS15b, JEH15, JEH16]. Several of these proposals have resulted in efficient algorithms with provable guarantees [CLS15b, CLS15a, JEH15]. However, such a multiple-shot experiment is largely impractical, as the specimen could be damaged before the measurement process is complete [SEC⁺15].

1.3 Holographic CDI and Holographic Phase Retrieval

In this paper, we consider another variant of CDI based on the holographic idea introduced by Gabor in 1948 [Gab48], which we shall term as *holographic CDI*. In holographic CDI, the experiment remains single-shot, but a “reference” area, whose structure is a priori known, is included in the diffraction area alongside the sample of interest (see Fig. 2 for the system setup and Fig. 3 for a schematic illustration).

Introducing a reference substantially simplifies the resulting phase retrieval problem, which we call *holographic phase retrieval*: the computational problem is now a linear deconvolution, which is equivalent to solving a linear system [KAKK72, ELS⁺04, GSF07, MA08, KH90]. The entailing computation can be further streamlined when certain specific reference shapes are employed. Due to its simplicity, holographic CDI is growing in its impact and popularity [GO18, SLLF12].

In the imaging community, popular reference choices are the pinhole reference [LU62, KH90], the slit reference [GSF07, GSF08, ZO10], and the block reference [PPP07, BSLL18, MA08], as illustrated in Fig. 4. Other proposed references include L-shapes [GSF07], parallelograms [GSF07], and annuluses [GO18], and

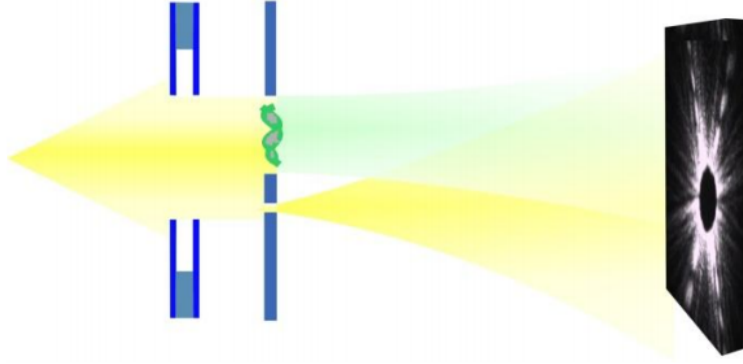


Figure 2: Holographic CDI setup. Image courtesy of [SLLF12].

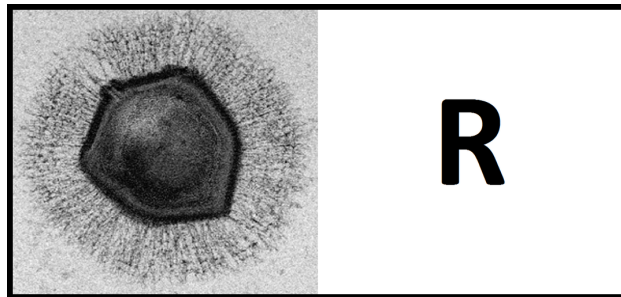


Figure 3: The diffraction area in Holographic CDI contains an unknown specimen (here shown as a mimivirus [GKL⁺08]) together with a known reference (here shown as “R”). Popular choices for the reference **R** are shown in Fig. 4.

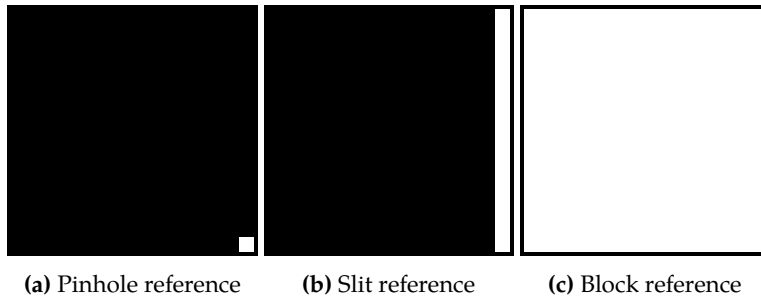


Figure 4: Schematic of the three leading reference choices for Holographic CDI. (Images have 16×16 enlarged pixels for illustration.)

Uniformly Redundant Arrays [MBS⁺08]. These reference shapes are typically realized as “empty space” cut out from a surrounding metal apparatus (see, e.g., Fig. 2). For signal recovery using these references, reference-specific algorithms—which take a different approach than linear deconvolution and only apply to small classes of references—have been proposed [GSF07]. Moreover, studies of these methods have to date been almost entirely empirical. Some error analysis is provided in [WTT⁺16].

1.4 Our Contributions

In this paper, we derive a general mathematical framework for holographic phase retrieval, encompassing the problem’s setup, recovery algorithm, and error analysis.

- Firstly, we formulate the holographic phase retrieval problem for a general specimen and reference setup. We then provide a recovery algorithm, termed Referenced Deconvolution, which essentially amounts to solving a structured linear system. We then further show how particular reference choices simplify this linear system. This provides a novel perspective on why fast, specialized algorithms (e.g., see [LU62, PPP07, GSF07]) can be designed for these reference choices.
- We derive a formula for the expected recovery error given noise-corrupted data. This formula offers a quantitative metric for experimental design and simulation, and allows for viewing the problem of reference design from an optimization perspective. This formula is then specialized to the Poisson shot noise, which occurs intrinsically in CDI due to quantum mechanical principles. This leads to the key notion of the *reference scaling factor*, based on which we characterize the popular references. In particular, the pinhole reference (Fig. 4a) is a good choice for “flat-spectrum” data, whereas the block reference (Fig. 4c) is well suited for low-frequency dominant data.

Numerical results demonstrate the power of the proposed referenced deconvolution method and the advantage of the block reference for recovering typical CDI imaging specimens. We also view this work as a means to introduce the holographic phase retrieval problem and the optimal reference design problem to a wider mathematical and scientific audience.

1.5 Paper Organization

Section 2 introduces the holographic phase retrieval problem and the referenced deconvolution algorithm. The special cases of popular reference choices are then further studied. Section 3 introduces an error analysis framework for holographic phase retrieval and the referenced deconvolution algorithm. This is further specialized to Poisson shot noise. The notion of a *reference scaling factor* is introduced, and is shown to play a key role in analyzing the expected Poisson noise error resulting from a given reference choice. Specific error analysis is then provided for popular reference choices, and is used to compare their performance. Section 4 presents the results of numerical simulations.

2 Holographic Phase Retrieval and Referenced Deconvolution

The phase retrieval problem is introduced in Section 2.1. The holographic phase retrieval problem and the Referenced Deconvolution algorithm are then introduced in Section 2.2 and Section 2.3, respectively. Then, the algorithm and resulting linear system are specialized to the three popular reference choices in Section 2.4.

2.1 The Phase Retrieval Problem

We consider the discrete two-dimensional phase retrieval problem. This discrete setting is manifested in practical CDI experiments, since CCD detectors can only take measurements at a finite number of pixel locations.

For a signal $X \in \mathbb{C}^{n_1 \times n_2}$, let \hat{X} be the size $m_1 \times m_2$ discrete Fourier transform of X given by

$$\hat{X}(k_1, k_2) = \sum_{t_1=0}^{n_1-1} \sum_{t_2=0}^{n_2-1} X(t_1, t_2) e^{-2\pi i(t_1 k_1/m_1 + t_2 k_2/m_2)}, \quad k_1 \in \{0, \dots, m_1 - 1\}, k_2 \in \{0, \dots, m_2 - 1\}. \quad (2.1)$$

Whenever $m_1 > n_1$ and $m_2 > n_2$, the Fourier transform is injective and is said to be *oversampled*. The mapping can also be compactly expressed as matrix multiplication:

$$\hat{X} = F_L X F_R^T, \quad (2.2)$$

where $F_L \in \mathbb{C}^{m_1 \times n_1}$ and $F_R \in \mathbb{C}^{m_2 \times n_2}$ are the corresponding discrete Fourier transform (DFT) matrices given by

$$F_L(k, t) = e^{-2\pi i k t / m_1} \quad \text{for } (k, t) \in \{0, \dots, m_1 - 1\} \times \{0, \dots, n_1 - 1\},$$

$$F_R(k, t) = e^{-2\pi i kt/m_2} \quad \text{for } (k, t) \in \{0, \dots, m_2 - 1\} \times \{0, \dots, n_2 - 1\}.$$

When $m_1 \geq n_2$ and $m_2 \geq n_2$, both F_L and F_R have mutually orthogonal columns, and so the inverse mapping is given simply by

$$X = \frac{1}{m_1 m_2} F_L^* \widehat{X} (F_R^*)^T. \quad (2.3)$$

The forward and inverse transforms in Eqs. (2.2) and (2.3) can also be conveniently expressed as a single matrix multiplication based on matrix Kronecker products. Let $\text{vec}(\cdot)$ be the columnwise vectorization operator acting on matrices and \otimes denote the matrix Kronecker products. The following result can be directly verified:

Lemma 2.1. $Y = AXB \iff \text{vec}(Y) = (B^T \otimes A) \text{vec}(X)$.

Applying Lemma 2.1 to Eqs. (2.2) and (2.3) gives

$$\text{vec}(\widehat{X}) = (F_R \otimes F_L) \text{vec}(X), \quad (2.4)$$

$$\text{vec}(X) = \frac{1}{m_2^2} (F_R^* \otimes F_L^*) \text{vec}(\widehat{X}), \quad \text{when } m_1 \geq n_1 \text{ and } m_2 \geq n_2. \quad (2.5)$$

We are now ready to define the phase retrieval problem in the two-dimensional, discrete setting.

Definition 2.2. *The (Fourier) phase retrieval problem consists of recovering a signal $X \in \mathbb{C}^{n_1 \times n_2}$ given the squared magnitudes of its Fourier transform values, i.e. given the set of values $|\widehat{X}(k_1, k_2)|^2, k_1 \in \{0, \dots, m_1 - 1\}, k_2 \in \{0, \dots, m_2 - 1\}$, which shall be denoted as $|\widehat{X}(k_1, k_2)|^2$.*

Here, exact recovery is not possible, as the mapping $X \mapsto |\widehat{X}|^2$ is not injective due to the following intrinsic ambiguities:

1. Global phase shift: if $X \mapsto |\widehat{X}|^2$, then $e^{i\theta} X \mapsto |\widehat{X}|^2$ for any $\theta \in [0, 2\pi)$;
2. Conjugate-flipping: if $X \mapsto |\widehat{X}|^2$, then $X' \mapsto |\widehat{X}|^2$ for $X' \in \mathbb{C}^{n_1 \times n_2}$ with $\overline{X'(n_1 - 1 - t_1, n_2 - 1 - t_2)} = X'(t_1, t_2)$ for all t_1, t_2 .

As well, circular shifts of X also produce the same set of measurements if no nonzero entries are shifted past the signal domain boundaries. This gives a third intrinsic ambiguity for signals X which have zero rows or columns at their boundaries. Taking all possible compositions of these operations forms a set (in fact, an equivalence class) of signals which are ‘‘physically equivalent’’ to X and have exactly the same magnitude measurements $|\widehat{X}|^2$. Thus, recovering X from $|\widehat{X}|^2$ shall be understood as recovery up to these symmetries.

Definition 2.3. *For signals $X_1, X_2 \in \mathbb{C}^{n_1 \times n_2}$ both indexed over $\{0, 1, \dots, n_1 - 1\} \times \{0, 1, \dots, n_2 - 1\}$, the cross-correlation $C_{[X_1, X_2]} \in \mathbb{C}^{(2n_1 - 1) \times (2n_2 - 1)}$ between X_1 and X_2 is defined as*

$$C_{[X_1, X_2]}(s_1, s_2) = \sum_{t_1=0}^{n_1-1} \sum_{t_2=0}^{n_2-1} X_1(t_1, t_2) \overline{X_2(t_1 - s_1, t_2 - s_2)}, \quad (2.6)$$

for $(s_1, s_2) \in \{-(n_1 - 1), \dots, n_1 - 1\} \times \{-(n_2 - 1), \dots, n_2 - 1\}$, where any $X_1(t_1, t_2)$ or $X_2(t_1 - s_1, t_2 - s_2)$ in the summands that are outside the valid index range are taken as 0.

When X_1 and X_2 are both equal to the same signal X , $C_{[X_1, X_2]}$ is known as the *autocorrelation* of X , and is denoted by A_X . Let \widehat{X} be the size $m_1 \times m_2$ Fourier transform of X . It is well-known that [OS09]

$$|\widehat{X}|^2 = \widehat{A_X}, \quad (2.7)$$

where

$$\begin{aligned} \widehat{A}_X &= F_{LA} A_X F_{RA}^T \quad \text{with } F_{LA} \in \mathbb{C}^{m_1 \times (2n_1-1)}, m_1 \geq 2n_1 - 1 \quad F_{RA} \in \mathbb{C}^{m_2 \times (2n_2-1)}, m_2 \geq 2n_2 - 1 \\ &\quad \text{and } F_{LA}(k, t) = e^{-2\pi i k t / m_1} \quad \forall (k, t) \in \{0, \dots, m_1 - 1\} \times \{-(n_1 - 1), \dots, n_1 - 1\}, \\ &\quad \text{and } F_{RA}(k, t) = e^{-2\pi i k t / m_2} \quad \forall (k, t) \in \{0, \dots, m_2 - 1\} \times \{-(n_2 - 1), \dots, n_2 - 1\}. \end{aligned} \quad (2.8)$$

Moreover, if $m_1 \geq 2n_1 - 1$ and $m_2 \geq 2n_2 - 1$, the mapping $A_X \mapsto \widehat{A}_X$ is injective, and hence A_X can be recovered from \widehat{A}_X , or equivalently $|\widehat{X}|^2$, by the corresponding inverse transform:

$$A_X = \frac{1}{m_1 m_2} F_{LA}^* |\widehat{X}|^2 (F_{RA}^*)^T. \quad (2.9)$$

Namely, A_X is uniquely determined from the $m_1 \geq 2n_1 - 1, m_2 \geq 2n_2 - 1$ uniform frequency sampling points. The entire frequency spectrum is in turn determined by taking the 2D discrete-time Fourier transform of A_X . Thus, any oversampling past the $m_1 = 2n_1 - 1, m_2 = 2n_2 - 1$ threshold provides no additional information.¹ This is in some sense the phase retrieval analogue of the Shannon sampling theorem [CESV15].

A powerful result by Hayes [Hay82] establishes that for all two- or higher-dimensional signals, excluding a set of Lebesgue measure zero, the only transformations on X which preserve $|\widehat{X}|^2$ are the physically equivalent symmetries discussed above. Thus, phase retrieval is generally well-posed in two or higher dimensions.

2.2 Holographic Phase Retrieval and Deconvolution

For simplicity of exposition, henceforth we focus on square $X \in \mathbb{C}^{n \times n}$. Suppose a reference $R \in \mathbb{C}^{n \times n}$ of the same size is situated on the right next to X , i.e., as illustrated in Fig. 3. This gives $[X, R] \in \mathbb{C}^{n \times 2n}$ defined by

$$[X, R](t_1, t_2) = \begin{cases} X(t_1, t_2) & t_2 \in \{0, \dots, n-1\} \\ R(t_1, t_2) & t_2 \in \{n, \dots, 2n-1\}. \end{cases}$$

We may assume without loss of generality that the magnitudes of the entries of X and R are within the interval $[0, 1]$. This convention has the physical interpretation of indicating the (average) *transmission coefficient* of the specimen at each pixel location. Roughly speaking, the transmission coefficient measures the fraction of incident electromagnetic radiation that is transmitted, rather than being reflected or absorbed and is a material property—Fig. 5 shows the transmission coefficient of polycarbonate at different photon energy levels. We shall subsequently consider reference setups that are physically realized as shapes cut from a surrounding opaque apparatus (i.e. consisting of metal that blocks all incident radiation). For the opaque part, the transmission coefficient is 0, whereas for the cut-out part the coefficient is 1.

In the above setting, the *holographic phase retrieval* problem is:

Holographic phase retrieval: given $R \in \mathbb{C}^{n \times n}$ and $|\widehat{[X, R]}|^2 \in \mathbb{R}^{m_1 \times m_2}$, recover $X \in \mathbb{C}^{n \times n}$.

Henceforth we assume $m_1 = m_2 = m$ with $m \geq 4n - 1$. We can then recover the autocorrelation of $[X, R]$, $A_{[X, R]}$, by taking the inverse Fourier transform on $|\widehat{[X, R]}|^2$. To see how the reference R helps to significantly simplify the subsequent retrieval problem, we can think over the autocorrelation process, referring to Fig. 6: in obtaining the autocorrelation sequence, we fix one copy of $[X, R]$, move around (in \mathbb{R}^2) another copy, and calculate and record the inner product of the overlapped region (if any) each time. When the overlap covers only part of R in one copy and only part of X in the other, the inner product value can be considered as a linear measurement of X . Since X contains only n^2 free variables, n^2 non-degenerate linear measurements provide sufficient information for recovering X . From Fig. 6, we can gather n^2 such measurements by taking one quadrant of the cross-correlation between X and R , which is one segment of $A_{[X, R]}$! Recovering X from the cross-correlation is a linear deconvolution problem.

¹This is true at least when there is no noise.

Filter Transmission

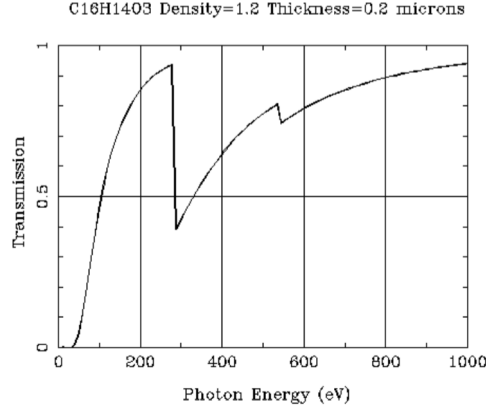


Figure 5: Transmission coefficient of polycarbonate at different photon energies [The10].

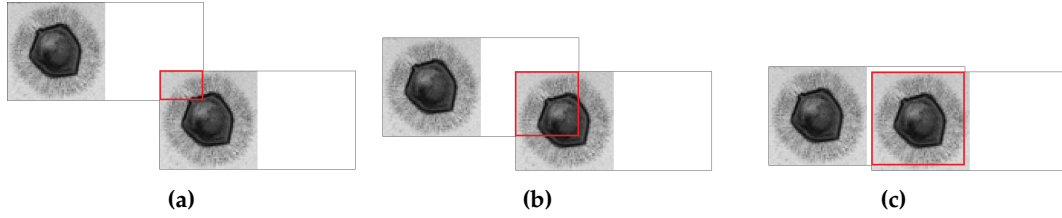


Figure 6: Near the boundary of the index range, each successive autocorrelation value of $[X, R]$ is formed by the overlap of a subregion of X with a subregion of R , which effectively gives a new linear measurement of X , as R is known. The original image X can then be recovered via solving the linear system in Eq. (2.12).

Extracting the desired cross-correlation from $A_{[X,R]}$ is as follows. For $(s_1, s_2) \in \{-(n-1), \dots, 0\} \times \{-(n-1), \dots, 0\}$,

$$\begin{aligned}
 C_{[X,R]}(s_1, s_2) &= \sum_{t_1=0}^{n-1} \sum_{t_2=0}^{n-1} X(t_1, t_2) \overline{R(t_1 - s_1, t_2 - s_2)} \\
 &= \sum_{t_1=0}^{n-1} \sum_{t_2=0}^{n-1} [X, R](t_1, t_2) \overline{[X, R](t_1 - s_1, t_2 + n - s_2)} \\
 &= \sum_{t_1=0}^{n-1} \sum_{t_2=0}^{2n-1} [X, R](t_1, t_2) \overline{[X, R](t_1 - s_1, t_2 + n - s_2)} \quad (\text{"zero-filling" rule in Definition 2.3}) \\
 &= A_{[X,R]}(s_1, -n + s_2).
 \end{aligned} \tag{2.10}$$

Since this is only a quadrant of the whole cross-correlation $C_{[X,R]}$, we shall write this part as $C_{[X,R]}^\diamond$. The above correspondence can be compactly written as

$$C_{[X,R]}^\diamond = P_1 A_{[X,R]} P_2^T, \tag{2.11}$$

where $P_1 = [I_n, 0_{n \times (n-1)}]$ and $P_2 = [I_n, 0_{n \times (3n-1)}]$.

For a fixed R , $C_{[X,R]}^\diamond$ is clearly linear in X . This linear relationship can be expressed conveniently as

$$\text{vec}(C_{[X,R]}^\diamond) = M_R \text{vec}(X), \tag{2.12}$$

for a corresponding matrix $M_R \in \mathbb{R}^{n^2 \times n^2}$, which can be constructed by inspection of Eq. (2.10). It is easy to verify that for any choice of R , M_R is lower-triangular and block-Toeplitz. We illustrate the form of M_R using a simple example.

Example 2.4. *Suppose*

$$R = \begin{bmatrix} r_{00} & r_{01} & r_{02} \\ r_{10} & r_{11} & r_{12} \\ r_{20} & r_{21} & r_{22} \end{bmatrix},$$

then

$$M_R = \begin{bmatrix} \overline{r_{22}} & 0 & 0 & 0 & 0 & 0 & 0 & 0 & 0 \\ \overline{r_{12}} & \overline{r_{22}} & 0 & 0 & 0 & 0 & 0 & 0 & 0 \\ \overline{r_{02}} & \overline{r_{12}} & \overline{r_{22}} & 0 & 0 & 0 & 0 & 0 & 0 \\ \overline{r_{21}} & 0 & 0 & \overline{r_{22}} & 0 & 0 & 0 & 0 & 0 \\ \overline{r_{11}} & \overline{r_{21}} & 0 & \overline{r_{12}} & \overline{r_{22}} & 0 & 0 & 0 & 0 \\ \overline{r_{01}} & \overline{r_{11}} & \overline{r_{22}} & \overline{r_{02}} & \overline{r_{12}} & \overline{r_{22}} & 0 & 0 & 0 \\ \overline{r_{20}} & 0 & 0 & \overline{r_{21}} & 0 & 0 & \overline{r_{22}} & 0 & 0 \\ \overline{r_{10}} & \overline{r_{20}} & 0 & \overline{r_{11}} & \overline{r_{21}} & 0 & \overline{r_{12}} & \overline{r_{22}} & 0 \\ \overline{r_{00}} & \overline{r_{10}} & \overline{r_{20}} & \overline{r_{01}} & \overline{r_{11}} & \overline{r_{21}} & \overline{r_{02}} & \overline{r_{12}} & \overline{r_{22}} \end{bmatrix}.$$

Note that M_R is invertible if and only if $R(n-1, n-1) \neq 0$. This invertibility condition is equivalent to the well-known ‘‘holographic separation condition’’ [GSF07], dictating when an image is recoverable via a reference object. Geometrically, it guarantees that there is no aliasing corrupting the cross-correlation.

Provided that $m \geq 4n - 1$ and $R(n-1, n-1) \neq 0$, we then have

$$\begin{aligned} \text{vec}(X) &= M_R^{-1} \text{vec}(C_{[X,R]}^\diamond) \\ &= M_R^{-1} \text{vec}(P_1 A_{[X,R]} P_2^T) \\ &= \frac{1}{m^2} M_R^{-1} \text{vec}(P_1 F_{LA}^* |\widehat{[X,R]}|^2 (F_{RA}^T)^* P_2^T), \end{aligned} \quad (2.13)$$

where $F_{LA} \in \mathbb{C}^{m \times (2n-1)}$ and $F_{RA} \in \mathbb{C}^{m \times (4n-1)}$ are centered DFT matrices, similar to those defined in Eq. (2.8).

Applying Lemma 2.1,

$$\text{vec}(X) = T_R \text{vec}(|\widehat{[X,R]}|^2), \quad (2.14)$$

where

$$T_R = \frac{1}{m^2} M_R^{-1} [(P_2 F_{RA}^*) \otimes (P_1 F_{LA}^*)]. \quad (2.15)$$

This gives a linear mapping between the squared Fourier transform magnitudes $|\widehat{[X,R]}|^2$ and the ground truth signal X .

2.3 Referenced Deconvolution

Combining Eqs. (2.13) and (2.14) gives an algorithm for recovering X given R and $Y \doteq |\widehat{[X,R]}|^2$. In practice, the measurements $|\widehat{[X,R]}|^2$ almost always contain noise, and we shall write the possibly noisy version as \tilde{Y} .

Algorithm 2.5 (Referenced Deconvolution for Holographic Phase Retrieval). *Let $X \in \mathbb{C}^{n \times n}$ be an unknown signal, $R \in \mathbb{C}^{n \times n}$ a known ‘‘reference’’ signal with $R(n-1, n-1) \neq 0$, and $Y \doteq |\widehat{[X,R]}|^2$ size $m \times m$ Fourier transform of $[X, R]$ with $m \geq 4n - 1$. Let \tilde{Y} be a noisy version of Y .*

1. Given \tilde{Y} , apply an inverse Fourier transform ($\mathbb{C}^{m \times m} \mapsto \mathbb{C}^{(2n-1) \times (4n-1)}$) to obtain $\widetilde{A_{[X,R]}}$, an estimate of the autocorrelation $A_{[X,R]}$;

2. Select the top-left $n \times n$ submatrix of $\widetilde{A}_{[X,R]}$, denoted as $\widetilde{C}_{[X,R]}^\circ$, which is an estimate of the top-left $n \times n$ quadrant of the cross-correlation $C_{[X,R]}$;
3. Set $\text{vec}(\widetilde{X}) = M_R^{-1} \text{vec}(\widetilde{C}_{[X,R]}^\circ)$.

Remark 2.6. If $\widetilde{Y} = Y$, then $\widetilde{X} = X$. In other words, [Algorithm 2.5](#) provides exact recovery in the noiseless setting.

2.4 Special Cases

We now specialize the referenced deconvolution algorithm to three popular reference choices: the pinhole reference, the slit reference, and the (constant) block reference (see [Fig. 4](#)). The different choices lead to different M_R 's in Step 3 of the algorithm. For all the three choices, the resulting M_R can be written as a Kronecker product of two simple matrices whose inverses are also explicit. To obtain explicit expressions for M_R^{-1} , we shall make use of the following fact.

Lemma 2.7 ([[TreND](#)]). *Suppose M_1 and M_2 are invertible. If $M = M_1 \otimes M_2$, then M is invertible and $M^{-1} = M_1^{-1} \otimes M_2^{-1}$.*

Thus, for $M_R = M_1 \otimes M_2$ with both M_1 and M_2 invertible, $M_R^{-1} = M_1^{-1} \otimes M_2^{-1}$. Invoking [Lemma 2.1](#) again, we conclude that Step 3 of the above referenced deconvolution algorithm becomes

$$\widetilde{X} = M_2^{-1} \widetilde{C}_{[X,R]}^\circ (M_1^{-1})^\top. \quad (2.16)$$

2.4.1 Pinhole Reference

Definition 2.8. *The pinhole reference $R_p \in \mathbb{C}^{n \times n}$ is given by*

$$R_p(t_1, t_2) = \begin{cases} 1, & t_1 = t_2 = n - 1 \\ 0, & \text{otherwise.} \end{cases} \quad (2.17)$$

It then follows that M_{R_p} is simply the identity matrix I_{n^2} (i.e., $I_n \otimes I_n$) and X is equal to $C_{[X,R]}^\circ$. Our referenced deconvolution algorithm reduces to the non-iterative reconstruction procedure for Fourier holography [[LU62](#)]. The deconvolution procedure thus has $O(1)$ computational complexity.

2.4.2 Slit Reference

Definition 2.9. *The slit reference R_s (see, e.g., [Fig. 4b](#)) is given by*

$$R_s(t_1, t_2) = \begin{cases} 1, & t_2 = n - 1 \\ 0, & \text{otherwise.} \end{cases} \quad (2.18)$$

Let $\mathbf{1}_L \in \mathbb{R}^{n \times n}$ be a lower-triangular matrix consisting of all ones on and below the main diagonal. It can be verified that

$$M_{R_s} = \text{diag}(\mathbf{1}_L, \dots, \mathbf{1}_L) = I_n \otimes \mathbf{1}_L. \quad (2.19)$$

The inverse of $\mathbf{1}_L$ is the first-order difference matrix [[Str16](#)]:

$$D_n(t_1, t_2) = \begin{cases} 1, & t_1 = t_2 \\ -1, & t_1 = t_2 - 1, \quad 1 \leq t_2 \leq n - 1 \\ 0, & \text{otherwise.} \end{cases} \quad (2.20)$$

Thus,

$$\widetilde{X} = D_n \widetilde{C}_{[X,R]}^\circ, \quad (2.21)$$

which only requires $O(n^2)$ operations to compute due to the sparsity structure of D_n .

2.4.3 Block Reference

Definition 2.10. The constant block reference R_b (see, e.g., Fig. 4c) is given by

$$R_b(t_1, t_2) = 1, \quad t_1, t_2 \in \{0, \dots, n-1\}. \quad (2.22)$$

The corresponding M_{R_b} is

$$M_{R_b} = \mathbf{1}_L \otimes \mathbf{1}_L, \quad (2.23)$$

and has inverse

$$M_{R_b}^{-1} = D_n \otimes D_n. \quad (2.24)$$

Thus,

$$\tilde{X} = D_n \widetilde{C_{[X,R]}} D_n^\top, \quad (2.25)$$

which as well is computed in $O(n^2)$ operations due to the sparsity structure of D_n .

On these special references, our referenced deconvolution algorithm is equivalent to the HERALDO procedure [GSF07]. We provide more details on the connection in Appendix A.

3 Error Analysis and Comparison

Let \tilde{Y} be the measurement data subject to certain stochastic noise and \tilde{X} be the estimate of the signal of interest returned by the referenced deconvolution algorithm. Hence, $\text{vec}(\tilde{X}) = T_R \text{vec}(\tilde{Y})$, where T_R is as defined in Eq. (2.15). This linear relationship allows us to derive a general formula for the expected squared recovery error in Section 3.1, which is then specialized for a Poisson shot noise model. We further simplify the error formula for the three reference choices listed in Section 3.2. This leads to insights regarding their recovery performance, which are discussed in Section 3.3.

3.1 Expected Error Formula

In dealing with complex-valued matrices, we use the standard Frobenius inner product as induced by the standard complex vector inner product.

Definition 3.1. For $B, C \in \mathbb{C}^{m \times m}$, their Frobenius (or, Hilbert-Schmidt) inner product is defined as $\langle B, C \rangle = \text{trace}(BC^*)$. The Frobenius matrix norm is induced by this inner product in a natural way: $\|B\|_F = (\langle B, B \rangle)^{1/2} = \left(\sum_{i,j} |B_{i,j}|^2 \right)^{1/2}$.

The following trace-shuffling identity is also useful for our subsequent calculation.

Lemma 3.2. For complex matrices B_1, B_2, C_1, C_2 of compatible dimensions, $\langle B_1 C_1, B_2 C_2 \rangle = \langle B_2^* B_1, C_2 C_1^* \rangle$.

We shall use this identity in obtaining a general formula for the expected squared recovery error.

Lemma 3.3. The expected squared recovery error given by the referenced deconvolution algorithm is

$$\mathbb{E} \left\| \tilde{X} - X \right\|_F^2 = \left\langle T_R^* T_R, \mathbb{E} \left[\text{vec}(\tilde{Y}) - \text{vec}(Y) \right] \left[\text{vec}(\tilde{Y}) - \text{vec}(Y) \right]^* \right\rangle, \quad (3.1)$$

where for any given reference R , T_R is as defined in Eq. (2.15).

Proof. Direct calculation gives

$$\mathbb{E} \left\| \tilde{X} - X \right\|_F^2 = \mathbb{E} \left\| T_R \text{vec}(\tilde{Y}) - T_R \text{vec}(Y) \right\|_F^2$$

$$\begin{aligned}
&= \mathbb{E} \left\langle T_R \text{vec}(\tilde{Y}) - T_R \text{vec}(Y), T_R \text{vec}(\tilde{Y}) - T_R \text{vec}(Y) \right\rangle \\
&= \mathbb{E} \left\langle T_R^* T_R, \left[\text{vec}(\tilde{Y}) - \text{vec}(Y) \right] \left[\text{vec}(\tilde{Y}) - \text{vec}(Y) \right]^* \right\rangle \\
&= \left\langle T_R^* T_R, \mathbb{E} \left[\text{vec}(\tilde{Y}) - \text{vec}(Y) \right] \left[\text{vec}(\tilde{Y}) - \text{vec}(Y) \right]^* \right\rangle,
\end{aligned}$$

as claimed. ■

This formula provides a very reasonable design target: given X and the noise model, one can seek a reference choice R which minimizes the expected squared error. This perspective forms the basis of our subsequent analysis.

We now specialize our analysis assuming a Poisson shot noise model on the data [Sch18]. Poisson shot noise occurs in any experiment in which photons are collected. It is an inherent feature of the quantum nature of photon emission, and cannot be removed by any physical apparatus [Sch18]. The model can be described as follows. Let N_p be the expected (or nominal) number of photons reaching the detector. Given the squared Fourier transform magnitudes $Y = |\widehat{[X, R]}|^2$, let

$$\|Y\|_1 \doteq \sum_{k_1, k_2=0}^{m-1} Y(k_1, k_2). \quad (3.2)$$

Then, the photon flux at the (k_1, k_2) -th pixel location is given by a Poisson distribution with parameter $N_p Y(k_1, k_2) / \|Y\|_1$ and then scaled by $\|Y\|_1 / N_p$. These pixel distributions are also assumed to be jointly independent [WTT⁺16]. We thus have the data given by

$$\tilde{Y} \sim \frac{\|Y\|_1}{N_p} \text{Pois} \left(\frac{N_p}{\|Y\|_1} Y \right). \quad (3.3)$$

We now apply this noise model to Eq. (3.1). Recall that both the mean and variance of a Poisson-distributed random variable with parameter λ are equal to λ . It then follows that ²

$$\begin{aligned}
\mathbb{E} \left[\text{vec}(\tilde{Y}) - \text{vec}(Y) \right] \left[\text{vec}(\tilde{Y}) - \text{vec}(Y) \right]^* &= \frac{\|Y\|_1^2}{N_p^2} \times \frac{N_p}{\|Y\|_1} \text{diag}(\text{vec}(Y)) \\
&= \frac{\|Y\|_1}{N_p} \text{diag}(\text{vec}(Y)).
\end{aligned}$$

Hence,

$$\mathbb{E} \|\tilde{X} - X\|_F^2 = \left\langle T_R^* T_R, \frac{\|Y\|_1}{N_p} \text{diag}(\text{vec}(Y)) \right\rangle = \frac{\|Y\|_1}{N_p} \langle S_R, Y \rangle, \quad (3.4)$$

where $S_R = \text{reshape}(\text{Diag}(T_R^* T_R), m, m)$, and $\text{reshape}(\cdot, m, m)$ is the columnwise vector-to-matrix reshaping operator. We shall term S_R the *reference scaling factor* corresponding to a reference R . Thus, the expected squared recovery error is proportional to the weighted sum of the squared frequency values in Y , where the weights are determined by S_R . S_R can be efficiently computed using the following observation.

Remark 3.4. For all $k_1, k_2 \in \{0, \dots, m-1\}$, let $k = mk_1 + k_2$. Then

$$S_R(k_1, k_2) = \|T_R(:, k)\|_2^2, \quad (3.5)$$

where $T_R(:, k)$ denotes the k^{th} column of T_R .

²We shall denote as $\text{diag}(\cdot)$ the operator that maps a vector to the corresponding diagonal matrix, and by $\text{Diag}(\cdot)$ the operator that maps the diagonal of a matrix to the corresponding vector.

Before we compute the S_R 's for the special references (i.e., [Section 3.2](#)), here we derive a (conservative) uniform lower bound on S_R .

Theorem 3.5. *For all reference choices R (with entry magnitudes normalized within $[0, 1]$), and for all $k_1, k_2 \in \{0, \dots, m-1\}$,*

$$S_R(k_1, k_2) \geq \frac{1}{m^4}. \quad (3.6)$$

Proof. For all $k_1, k_2 \in \{0, \dots, m-1\}$ and the corresponding $k = mk_1 + k_2$,

$$\begin{aligned} S_R(k_1, k_2) &= \|T_R(:, k)\|_2^2 \\ &= |T_R(0, k)|^2 + \sum_{t=1}^{n^2-1} |T_R(t, k)|^2 \\ &= \frac{1}{m^4} |(M_R^{-1} [(P_2 F_{RA}^*) \otimes (P_1 F_{LA}^*)]) (0, k)|^2 + \sum_{t=1}^{n^2-1} |T_R(t, k)|^2. \end{aligned}$$

By [Lemma 2.7](#), M_R^{-1} is lower triangular. So $(M_R^{-1} [(P_2 F_{RA}^*) \otimes (P_1 F_{LA}^*)]) (0, k)$ is equal to the product of $M_R^{-1}(0, 0)$, and the first element of the k -th column of $(P_2 F_{RA}^*) \otimes (P_1 F_{LA}^*)$ which takes the form $e^{i\theta}$ for a certain θ . Thus,

$$|(M_R^{-1} [(P_2 F_{RA}^*) \otimes (P_1 F_{LA}^*)]) (0, k)|^2 = |M_R^{-1}(0, 0)|^2 \geq 1, \quad (3.7)$$

where the last inequality holds, as we assume $M_R(0, 0) \in [0, 1]$. This completes the proof. \blacksquare

3.2 Special Cases

For the special cases, we shall see that T_R takes the form of $B_1 \otimes B_2$ for certain matrices B_1 and B_2 , which motivates the following result.

Lemma 3.6. *Suppose $B_1 \in \mathbb{C}^{n_1 \times m_1}$, $B_2 \in \mathbb{C}^{n_2 \times m_2}$, and $B = B_1 \otimes B_2 \in \mathbb{C}^{n_1 n_2 \times m_1 m_2}$. Then, for $k_1 \in \{0, \dots, m_1\}$, $k_2 \in \{0, \dots, m_2\}$, and $k = m_2 k_1 + k_2 \in \{0, \dots, m_1 m_2 - 1\}$, it holds that*

$$\|B(:, k)\|^2 = \|B_1(:, k_1)\|^2 \|B_2(:, k_2)\|^2.$$

Proof. By the definition of Kronecker product,

$$B(:, k) = \begin{bmatrix} B_1(0, k_1) B_2(:, k_2) \\ B_1(1, k_1) B_2(:, k_2) \\ \vdots \\ B_1(n_1, k_1) B_2(:, k_2) \end{bmatrix}.$$

Thus,

$$\|B(:, k)\|^2 = \sum_{t=0}^{n_1} |B_1(t, k_1)|^2 \|B_2(:, k_2)\|^2 = \|B_2(:, k_2)\|^2 \sum_{t=0}^{n_1} |B_1(t, k_1)|^2 = \|B_2(:, k_2)\|^2 \|B_1(:, k_1)\|^2,$$

as claimed. \blacksquare

Next, we make use of the result to calculate the expected recovery errors of the special references as introduced in [Section 2.4](#).

3.2.1 Pinhole Reference

Theorem 3.7. Let R_p denote the pinhole reference given by [Definition 2.8](#). For $k_1, k_2 \in \{0, \dots, m-1\}$,

$$S_{R_p}(k_1, k_2) = \frac{n^2}{m^4}. \quad (3.8)$$

Proof. Since $M_{R_p} = I_{n^2}$, by [Eq. \(2.14\)](#), we have that

$$T_{R_p} = \frac{1}{m^2} (P_2 F_{RA}^*) \otimes (P_1 F_{LA}^*).$$

By [Remark 3.4](#) and [Lemma 3.6](#), for any $k_1, k_2 \in \{0, \dots, m-1\}$ and $k = mk_1 + k_2$,

$$S_{R_p}(k_1, k_2) = \frac{1}{m^4} \|(P_2 F_{RA}^*)(:, k_1)\|^2 \|(P_1 F_{LA}^*)(:, k_2)\|^2.$$

Observing that any element in $P_2 F_{RA}^*$ or $P_1 F_{LA}^*$ has a unit norm, we conclude that

$$\|(P_2 F_{RA}^*)(:, k_1)\|^2 = \|(P_1 F_{LA}^*)(:, k_2)\|^2 = n,$$

implying the claimed result. ■

3.2.2 Slit Reference

Theorem 3.8. Let R_s denote the slit reference given by [Definition 2.9](#). For $k_1, k_2 \in \{0, \dots, m-1\}$,

$$S_{R_s}(k_1, k_2) = \frac{n}{m^4} [1 + 2(n-1)(1 - \cos(2\pi k_2/m))].$$

Proof. By the discussion below [Definition 2.9](#),

$$M_{R_s}^{-1} = I_n \otimes D_n,$$

where D_n is the first-order difference matrix defined in [Eq. \(2.20\)](#). So by [Eq. \(2.14\)](#),

$$T_{R_s} = \frac{1}{m^2} [I_n \otimes D_n] ((P_2 F_{RA}^*) \otimes (P_1 F_{LA}^*)) = (P_2 F_{RA}^*) \otimes (D_n P_1 F_{LA}^*),$$

where in the last equality we have used the ‘‘mixed-product’’ property of Kronecker products³.

By [Remark 3.4](#) and [Lemma 3.6](#), for any $k_1, k_2 \in \{0, \dots, m-1\}$ and $k = mk_1 + k_2$,

$$S_{R_s}(k_1, k_2) = \frac{1}{m^4} \|(P_2 F_{RA}^*)(:, k_1)\|^2 \|(D_n P_1 F_{LA}^*)(:, k_2)\|^2.$$

Per the proof of [Theorem 3.7](#), $\|(P_2 F_{RA}^*)(:, k_1)\|^2 = n$. For the other term,

$$\begin{aligned} \|(D_n P_1 F_{LA}^*)(:, k_2)\|^2 &= \|D_n P_1 [F_{LA}^*(:, k_2)]\|^2 \\ &= \left\| D_n \begin{bmatrix} e^{-2\pi i(n-1)k_2/m} \\ e^{-2\pi i(n-2)k_2/m} \\ \vdots \\ e^{2\pi i 0 k_2/m} \end{bmatrix} \right\|^2 \\ &= 1 + \sum_{t=1}^{n-1} \left| e^{-2\pi i t k_2/m} - e^{-2\pi i (t-1)k_2/m} \right|^2 \\ &= 1 + \sum_{t=1}^{n-1} (2 - 2 \cos(2\pi k_2/m)) \\ &= 1 + 2(n-1)(1 - \cos(2\pi k_2/m)), \end{aligned}$$

completing the proof. ■

³This is the fact that $(A \otimes B)(C \otimes D) = (A \otimes C)(B \otimes D)$ for matrices A, B, C, D of compatible dimensions.

3.2.3 Block Reference

Theorem 3.9. Let R_b denote the block reference given by [Definition 2.10](#). For $k_1, k_2 \in \{0, \dots, m-1\}$,

$$S_{R_b}(k_1, k_2) = \frac{1}{m^4} [1 + 2(n-1)(1 - \cos(2\pi k_1/m))] [1 + 2(n-1)(1 - \cos(2\pi k_2/m))]. \quad (3.9)$$

Proof. As shown in [Eq. \(2.24\)](#),

$$M_{R_b}^{-1} = D_n \otimes D_n.$$

After applying the mixed-product property of the Kronecker product and also [Lemma 3.6](#) analogously to the above proof of the slit reference, it is clear that we only have to calculate $\|(D_n P_1 F_{LA}^*)(:, k_2)\|^2$ and $\|(D_n P_2 F_{RA}^*)(:, k_1)\|^2$. Performing analogous calculation as in the slit reference case then completes the proof. \blacksquare

Note that S_{R_b} achieves the uniform lower bound (i.e., $1/m^4$) around $k_1 = k_2 = 0$.

3.3 Reference Design Optimality

For a fixed specimen X , we may view the recovery error given by [Eq. \(3.4\)](#) as an objective (i.e. cost) function whose variables are the reference values. From this perspective, each of the special cases considered exhibits a unique characteristic, as we discuss below.

Note that these observations describe how the reference scaling factor S_R depends on the reference choice R . This only partially describes the effect of the reference choice R on the expected error given in [Eq. \(3.4\)](#). Of course, the choice of R will also affect Y itself. However, the effect of R on the former will typically far outweigh the latter by several orders of magnitude. We provide a sketch argument explaining this below.

In [Eq. \(3.4\)](#), both $Y = \|\widehat{[X, R]}\|^2$ and S_R depend on the reference R , and both Y and S_R contribute to the expected error.

- For Y , note that

$$\|\widehat{[X, R]}\|^2 = \|\widehat{[X, 0]}\|^2 + \|\widehat{[0, R]}\|^2 \quad (\text{Fourier transform is a linear operator}) \quad (3.10)$$

$$= \|\widehat{[X, 0]}\|^2 + \|\widehat{[0, R]}\|^2 + 2\Re\left(\widehat{[X, 0]} \odot \widehat{[0, R]}\right), \quad (3.11)$$

where \odot denotes the elementwise Hadamard product. Moreover,

$$\|Y\|_1 = \|\widehat{[X, R]}\|_F^2 = m^2 \|[X, R]\|_F^2 = m^2 \|X\|_F^2 + m^2 \|R\|_F^2, \quad (3.12)$$

where the second equality follows from Parseval's theorem.

- The S_R term changes significantly across the references: for example, on a 64×64 image, the zero-frequency scaling term $S_R(0, 0)$ for the block reference is $1/64$ of that for the slit reference, and is $1/64^2$ of that for the pinhole reference, as implied by [Theorems 3.7 to 3.9](#). By [Theorem 3.7](#), the pinhole reference induces a “flat” weighting scheme with a uniform weight n^2/m^4 . By contrast, the weights induced by the block reference are frequency-varying ([Theorem 3.9](#)): when one of k_1 and k_2 is reasonably small, the weights are on the order $O(n/m^4)$, and when both are small, the weights are on the optimal order $O(1/m^4)$, which matches the lower bound given by [Theorem 3.5](#). The weights induced by the slit reference interpolate the previous two in different directions: for a fixed k_2 , the weight is constant and the behavior matches that of the pinhole reference, whereas the behavior is similar to that of the block reference when k_2 changes. The weighting behaviors of the three references are demonstrated in [Fig. 7](#).

To illustrate how [Eq. \(3.4\)](#) and the above facts can help provide insights into reference design and choice, we look at two stylized cases. For this discussion, reference choice is confined to the three special references we discussed above.

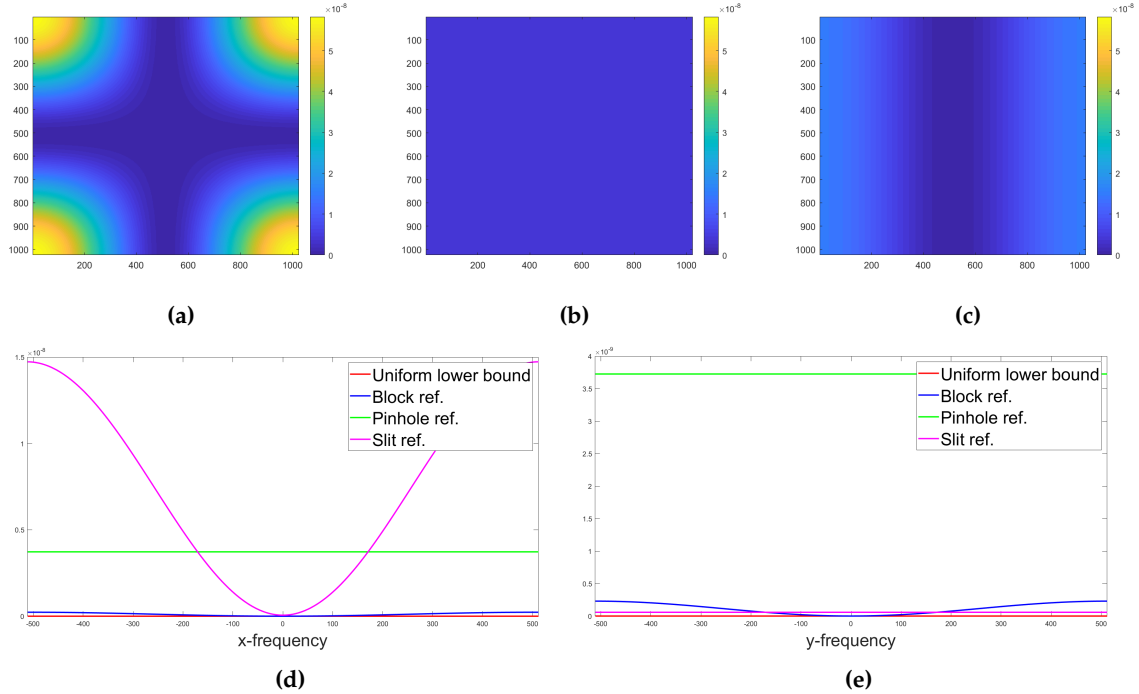


Figure 7: Plot of S_R for the three special references and the uniform lower bound established in [Theorem 3.5](#). [Fig. 7a](#), [Fig. 7b](#), [Fig. 7c](#) show the S_R for the block, pinhole, and slit references, respectively. [Fig. 7d](#) and [Fig. 7e](#) show the cross-sections cutting the origin and parallel to the x and y directions, respectively. While the pinhole reference induces a flat scaling to the entire spectrum (as predicted in [Theorem 3.7](#)), the values for the block references are small at the low frequencies, and grow toward larger values moving into high frequencies. The slit reference interpolates the behaviors across directions: along the y -axis, the values are constant—same as the pinhole reference, but along the x -axis, the value increases as the frequency grows, similarly to the block reference.

- **Case I: Spectrum of X concentrates on (super) low-frequency bands.** A good example is when $X = \mathbf{1}_{n \times n}$. We think of X as “flat” and has values on the order of $\Theta(1)$. So $\|X\|_F^2 \in \Theta(n^2)$. Then whatever the choice of R , $\|X\|_F^2 + \|R\|_F^2 \in \Theta(n^2)$. So the contribution by $\|Y\|_1$ only differs across the three references by a small constant factor. Moreover, by [Eq. \(3.10\)](#), Y is low-frequency dominant regardless of the reference. According to our above discussion about the weight distribution of S_R , using the block reference might be beneficial for this class of signals (depending on of course how concentrated the low-frequency components of Y is).
- **Case II: Spectrum of X is flat or has significant medium- to high-frequency components.** An idealized example is when $X = \delta(0, 0)$, and we focus on the pinhole and block references. For either of them, the medium- to high-frequency components in S_R are on the same order (i.e., $O(n^2/m^4)$ from [Theorem 3.7](#) and [Theorem 3.9](#)), and in Y are on the same order also (i.e., $O(1)^4$). For the low-frequency part, S_{R_b} are $O(1/m^4)$, and S_{R_p} are $O(n^2/m^4)$. Moreover, for the low-frequency part of Y , $|\widehat{[X, R_b]}|^2$ are dominated by $|\widehat{[0, R_b]}|^2$, which is $O(n^2)$, and $|\widehat{[X, R_p]}|^2$ are $O(1)$. Thus, $\langle S_R, Y \rangle$ are on the same order whether we choose the block or the pinhole reference. So the final performance of the two is largely determined by $\|Y\|_1$. When $\|X\|_F \in o(n^2)$, say $\|X\|_F = 1$ (for $\delta(0, 0)$), obviously the pinhole reference is

⁴Recall we focus on the medium- to high-frequency spectrum part here. This part for $|\widehat{[X, 0]}|^2$ are all ones if $X = \delta(0, 0)$. Moreover, when $R = R_p$, both $|\widehat{[0, R]}|^2$ and $2\Re[\widehat{X, 0}] \odot \widehat{[0, R]}$ are $O(1)$. When $R = R_b$, this part for $|\widehat{[0, R]}|^2$ are also $O(1)$ in magnitude (think of the quick decay behavior of the sinc function), and hence $2\Re[\widehat{X, 0}] \odot \widehat{[0, R]}$ are $O(1)$ as well.

more favorable, as $\|R_p\|_F^2 = 1$ whereas $\|R_b\|_F^2 = n^2$. But if $\|X\|_F^2 \in \Theta(n^2)$, we do not expect substantial differences.

It is natural to expect a smooth transition of the behaviors moving from the super-flat signal $\mathbf{1}_{n \times n}$ to the super sharp $\delta(0, 0)$. We confirm the differential behaviors of the references empirically in [Section 4](#).

3.4 Error Perturbation

Our error formula [Eq. \(3.4\)](#) gives only the expected squared recovery error, and our results in [Section 3.2](#) and particularly the optimality analysis in [Section 3.3](#) are derived based on this expected error. One may wonder if it is reasonable to base the analysis solely on expectation. The following perturbation bound provides some insights in this direction.

Theorem 3.10. *For each of the pinhole, slit, and block references, and for the Poisson noise model on \tilde{Y} given by [Eq. \(3.3\)](#), the following holds. For all $t > 0$,*

$$\mathbb{P} \left[\left| \|\tilde{X} - X\|_F^2 - \mathbb{E} \|\tilde{X} - X\|_F^2 \right| \geq t \right] \leq 2 \exp \left\{ -c \min \left(\frac{N_p m t^{1/2}}{\sqrt{3N_p} \|Y\|_1 \|Y\|_\infty + 2 \|Y\|_1}, \frac{N_p^4 m^4 t^2}{n^2 (\sqrt{3N_p} \|Y\|_1 \|Y\|_\infty + 2 \|Y\|_1)^4} \right) \right\}, \quad (3.13)$$

where $c > 0$ is a universal constant.

Proof of this theorem is included in [Appendix B](#). To make sense of this theorem, let us plug in some practical values for the parameters: $t = n^2 t_0$ (i.e., t_0 is the average pixel-wise perturbation), $N_p = C_0 m^2$ for a large constant C_0 , $\|Y\|_1$ is typically $O(m^2 n^2)$ and $\|Y\|_\infty$ is typically $O(n^2)$ (i.e., the spectrum is not too peaky). Then we have

$$\frac{N_p m t^{1/2}}{\sqrt{3N_p} \|Y\|_1 \|Y\|_\infty + 2 \|Y\|_1} = c_1 C_0 \frac{m}{n} t_0^{1/2}, \quad (3.14)$$

$$\frac{N_p^4 m^4 t^2}{n^2 (\sqrt{3N_p} \|Y\|_1 \|Y\|_\infty + 2 \|Y\|_1)^4} = c_2 C_0^4 \frac{m^4}{n^6} t_0^2. \quad (3.15)$$

Evidently, making C_0 large and m large (relative to n) improves the concentration. For example, in our experiment below, $C_0 \gg 100 > n$ and $m \geq 10n$, making the above exponents reasonably large and hence the tail probability negligibly small even for small t_0 .

4 Numerical Simulations

We perform numerical experiments on two sets of data to illustrate the effectiveness of the referenced deconvolution algorithm ([Section 2.3](#)), and to corroborate the theoretical prediction on optimal reference design ([Section 3.3](#)). Codes for these experiments are available at https://github.com/sunju/REF_CDI.

4.1 On the Mimivirus Image

In this experiment, the specimen X is the mimivirus image [[GKL⁺08](#)], and its spectrum mostly concentrates on very low frequencies, as shown in [Fig. 10b](#). The image size is 64×64 , and the pixel values are normalized to $[0, 1]$. For the referenced setup, a reference R of size 64×64 is placed next to X , forming a composite specimen $[X, R]$ of size 64×128 . Three references, i.e., the pinhole, the slit, and the block references are considered. The oversampled Fourier transform is taken to be of size 1024×1024 , and the collected noisy data \hat{Y} obeys the Poisson shot noise model defined in [Eq. \(3.3\)](#). For this model, the nominal number of total photons N_p is

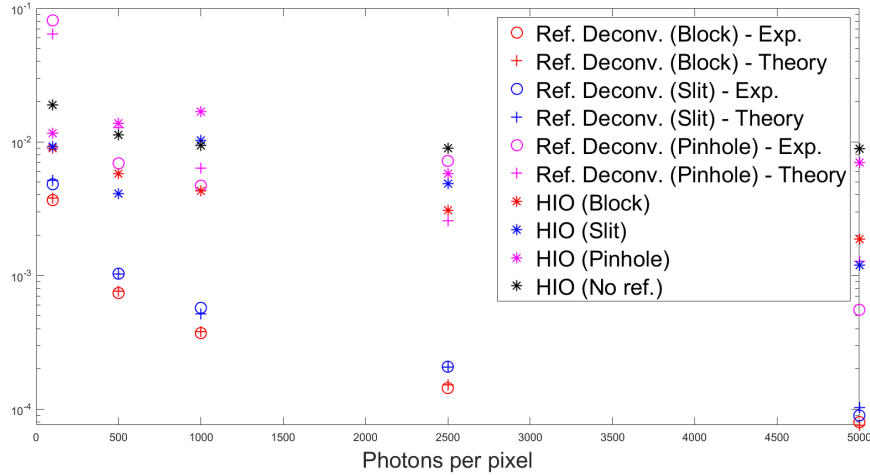


Figure 8: Plot of the relative recovery error against the nominal photon level for experiments on the mimivirus image. Result from both the referenced deconvolution and the classic HIO algorithms are included. For the referenced deconvolution algorithm, both the expected and empirical recovery errors are presented. The referenced deconvolution algorithm combined with the block reference performs consistently better than other algorithm-reference combinations. Also, for each reference, the expected recovery error closely matches the empirical recovery error, as predicted by [Theorem 3.10](#).

given by $N_{pp} \times 1024^2$, where N_{pp} can be understood to be the average number of photons to be received by each pixel. We investigate the regime where N_{pp} varies from 100 to 5000 ($N_{pp} = 100, 500, 1000, 2500, 5000$, respectively), with one simulation trial run for each N_{pp} value.

We run the referenced deconvolution algorithm and also the classic HIO algorithm with and without enforcing the known reference for comparison. The results are presented in [Fig. 8](#) and [Fig. 9](#). We define the relative (squared) recovery error to be

$$\varepsilon \doteq \frac{\|X - \hat{X}\|^2}{\|X\|^2}. \quad (4.1)$$

From [Fig. 8](#), it is evident that for the referenced deconvolution schemes, the expected and empirical relative recovery errors are close (justified by the perturbation result in [Section 3.4](#)). Moreover, referenced deconvolution combined with the block reference performs the best among all the algorithm and reference combinations—regardless of the photon per pixel level N_{pp} . The superiority of the block reference among the referenced deconvolution schemes agrees with the prediction in [Section 3.3](#), as the spectrum of X sharply concentrates on very low frequencies. In addition, for the referenced deconvolution schemes, the recovery errors generally decrease as the photon level (dictated by N_{pp}) increases. This trend is clearly predicted by [Eq. \(3.4\)](#): because only $N_p = N_{pp} \times 1024^2$ depends on N_{pp} , the expected squared error is proportional to $1/N_{pp}$. The relative errors and recovered images for $N_{pp} = 1000$ are exhibited in [Fig. 9](#).

In regards to algorithm runtime for our experiments, the referenced deconvolution algorithm runs in less than 0.001 seconds for all three reference choices considered. The runtime for HIO is about 0.2 seconds per iteration, with the iteration with the smallest relative error selected from 1000 iterations.

4.2 On a “Flat-Spectrum” Image

In this experiment, the image contains a small centered square. Except for this, the basic experimental setup is identical to the above one. We focus on the case $N_{pp} = 1000$. In terms of recovery error, the referenced

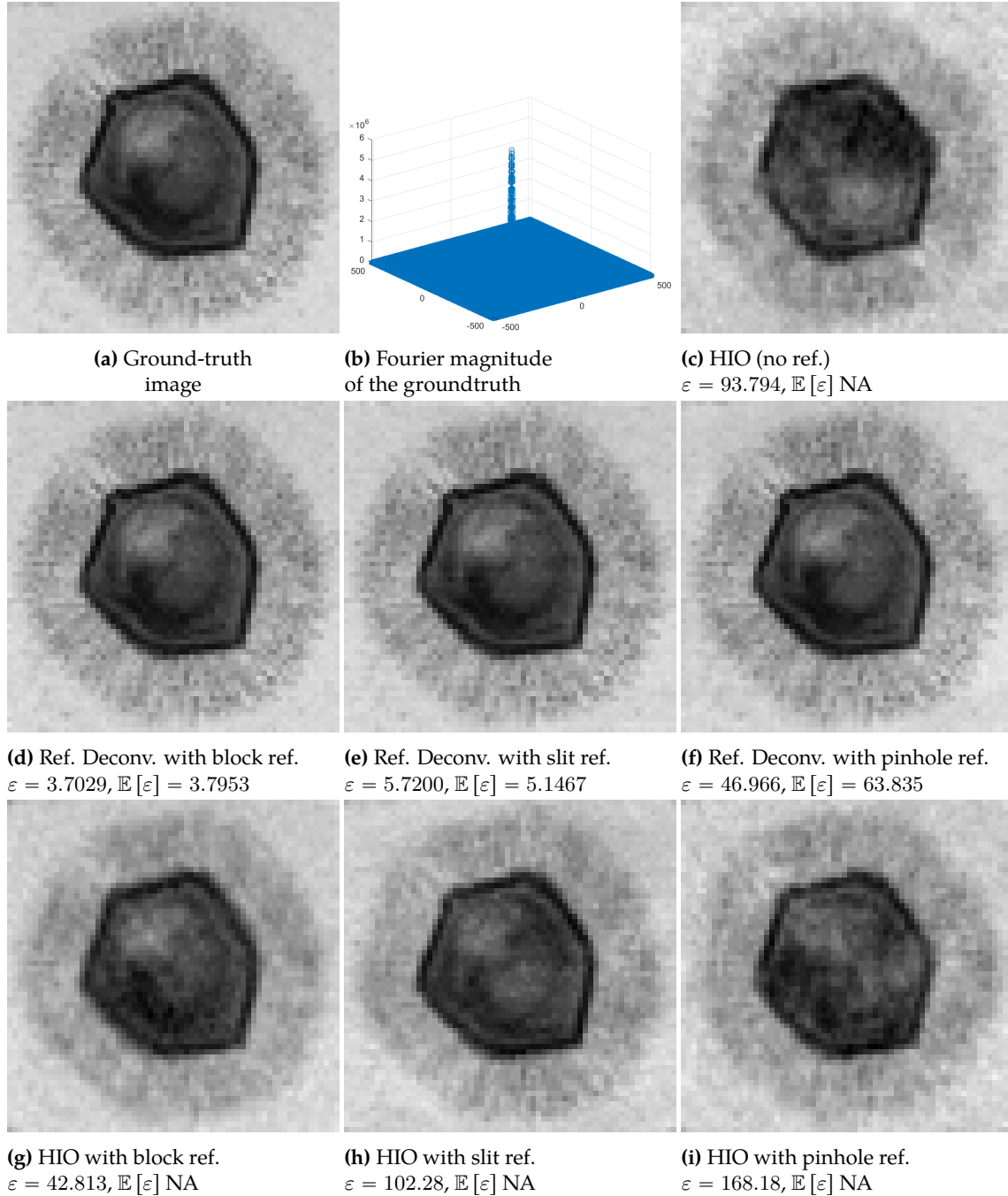


Figure 9: Recovery result of the mimivirus image using various recovery schemes, and the corresponding relative recovery errors (**all errors should be rescaled by 10^{-4}**). The photon level is fixed at $N_{pp} = 1000$. Referenced deconvolution achieves superior recovery to HIO, both with and without the reference information enforced. Experimental and theoretical relative errors for referenced deconvolution closely match, as predicted by [Theorem 3.10](#). The block reference achieves the best recovery.

deconvolution schemes perform uniformly better than the HIO schemes, just as for the mimivirus image. For the current “centered square” image which has a considerably “flat” spectrum (see [Fig. 10b](#)), however,

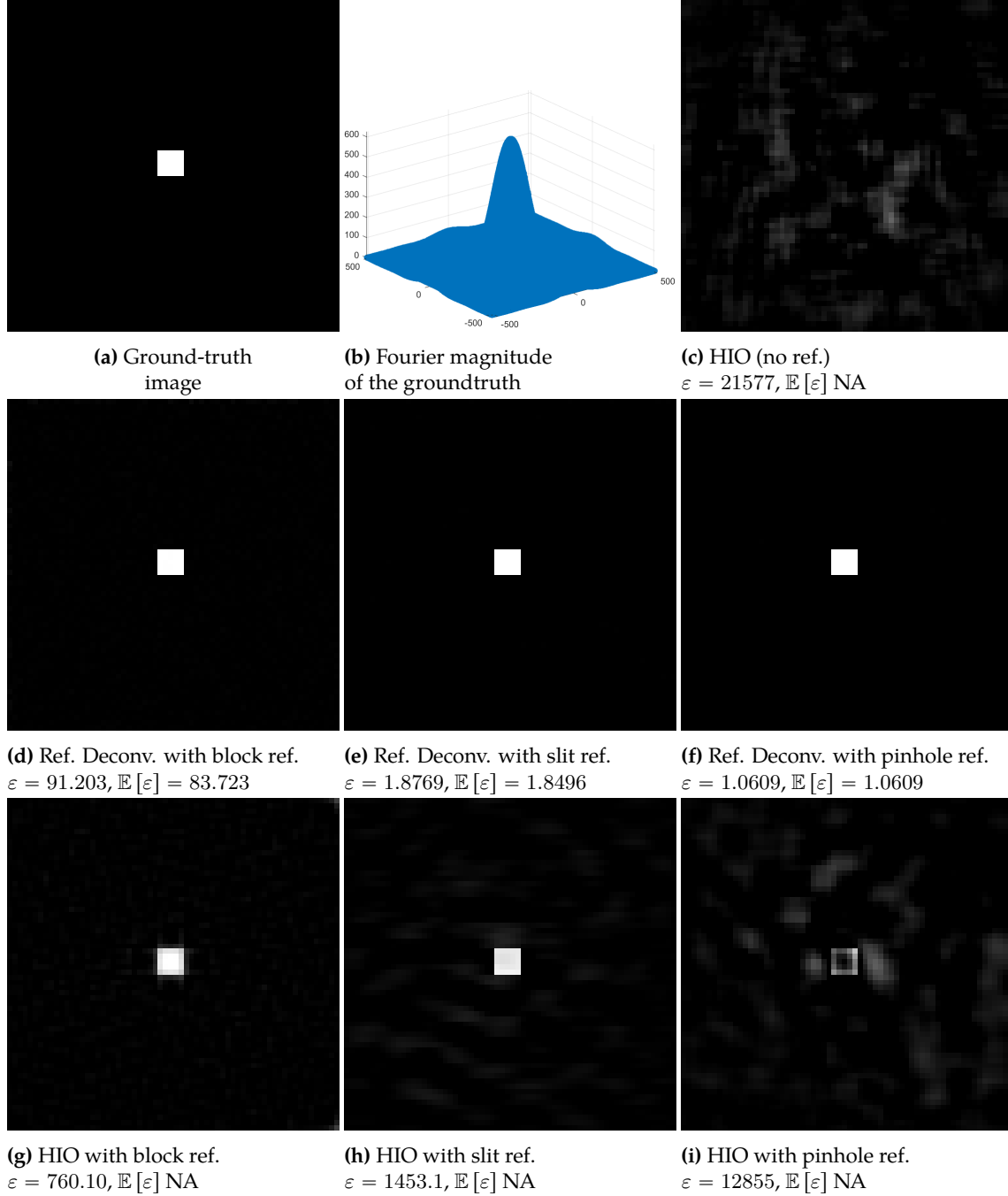


Figure 10: Recovery result of the “centered square” image using various recovery schemes, and the corresponding relative recovery errors (**all errors should be rescaled by 10^{-4}**). The photon level N_{pp} is fixed as 1000. Referenced deconvolution achieves superior recovery to HIO (with the reference information enforced). Experimental and theoretical relative errors for referenced deconvolution closely match, as predicted by [Theorem 3.10](#). The pinhole reference achieves the best recovery.

the best-performing reference is the pinhole reference—again consistent with our theoretical prediction in [Section 3.3](#). The detailed recovery results and recovery errors are presented in [Fig. 10](#).

5 Discussion

We have presented a general mathematical framework for the holographic phase retrieval problem, and proposed the referenced deconvolution algorithm as a generic solution scheme. Our formulation emphasizes the structure in the linear deconvolution procedure, and offers new insights into the resulting linear systems from popular reference choices.

We have also derived a general formula for the expected recovery error of the referenced deconvolution algorithm when the measurement data contains stochastic noise. Under a Poisson shot noise model, the formula allows us to compare popular reference choices and conclude that the block reference minimizes low-frequency contributions to the recovery error and is hence favorable for typical imaging data.

Building on our framework, it is possible to perform more detailed analysis of other noise models and reference choices. Also, the insights obtained here can likely motivate further design possibilities. In our follow-up work [BSC⁺19], one such new reference setup (termed the *dual-reference*) is proposed, which provides superior noise stability across the frequency spectrum, as compared to popular single-reference setups.

Another possible extension is to include beamstops, which are often implemented in practical CDI experiments [GSF07, HSC15]. Beamstops effectively remove a small fraction ($\leq 5\%$) of low-frequency components from the measurements. We observe that the proposed referenced deconvolution algorithm is easily adapted to this setting, insofar as the missing data does not render the problem ill-conditioned.

6 Acknowledgments

The authors are grateful to the Simons Foundation Math+X initiative and the Natural Science and Engineering Research Council of Canada for providing support during our study. We would also like to sincerely thank Walter Murray, Gordon Wetzstein, and Jon Claerbout for ongoing valuable feedback towards developing this work.

A Connection with HERALDO

We sketch the correspondence between the Referenced Deconvolution algorithm and the HERALDO procedure [GSF07].

A.1 Summary of HERALDO

The HERALDO procedure (an acronym for ‘‘Holography with Extended Reference by Autocorrelation Linear Differential Operation’’) considers a continuous setup with a specimen $X(x, y)$ and reference $R(x, y)$ which together form the composite $F(x, y) = X(x, y) + R(x, y)$. Let \star denote the cross-correlation. It follows that

$$F \star F = X \star X + R \star R + X \star R + R \star X. \quad (\text{A.1})$$

Provided that R and X satisfy certain separation conditions, the cross-correlation $R \star X$ will not overlap with the other terms in Eq. (A.1). The HERALDO idea is to find an n^{th} order weighted linear differential operator \mathcal{L}_R^n , i.e.,

$$\mathcal{L}_R^n = \sum_{k=0}^n a_k \frac{\partial^n}{\partial x^{n-k} \partial y^k}, \quad \text{where } a_k\text{'s are the weights,} \quad (\text{A.2})$$

such that

$$\mathcal{L}_R^n(R) = A\delta(x - x_0, y - y_0) + o(x, y), \quad (\text{A.3})$$

for some constants A, x_0, y_0 and some offset function $o(x, y)$. Now, applying the key identities

$$\mathcal{L}^{(n)}(h \star g) = \mathcal{L}^{(n)}(h) \star g = (-1)^n h \star \mathcal{L}^{(n)}(g) \quad \forall h, g, \quad (\text{A.4})$$

one can show that

$$\begin{aligned} \mathcal{L}_R^{(n)}(F * F) &= \mathcal{L}_R^{(n)}(X \star X) + \frac{1}{2} [AR^*(x_0 - x, y_0 - x) + o \star R] + (-1)^n \frac{1}{2} [A^*R(x_0 + x, y_0 + x) + R \star o] + \\ &\quad (-1)^n o \star X + X \star o + (-1)^n A^*X(x + x_0, y + y_0) + AX^*(x_0 - x, y_0 - y). \end{aligned}$$

Appropriate separation conditions on the supports (i.e., domains of nonzeros) of X, R , and o then ensure either $A^*X(x + x_0, y + y_0)$ or $AX^*(x_0 - x, y_0 - y)$ be separate from other terms spatially. This provides a scaled and shifted copy of X , thereby recovering the unknown specimen of interest.

Note that for an arbitrary reference R , determining whether such an \mathcal{L}_R^n exists and how it can be constructed is a highly nontrivial problem. Nonetheless, for special references such as the pinhole, slit, and block, there are easy constructions as illustrated in [GSF07].

A.2 Connection to the Referenced Deconvolution Algorithm

The HERALDO procedure seeks a continuous linear differential operator \mathcal{L}_R^n such that $\mathcal{L}_R^n(R) = A\delta(x - x_0, y - y_0) + o(x, y)$. Consider the special case where $A = 1, x_0 = y_0 = 0$, and $o(x, y) = 0$, whence

$$\mathcal{L}_R^n(R) = \delta(x, y). \quad (\text{A.5})$$

The paper [GSF07] has derived the respective linear differential operators with $n \leq 2$ for the pinhole, slit, and block references. For each of these three special references, we observe that M_R^{-1} is exactly a finite-difference approximation to the linear differential operator derived in [GSF07]⁵, which is elaborated below.

A.2.1 Pinhole Reference

For the pinhole reference R_p , $\mathcal{L}_{R_p}^n$ is simply the identity operator, and hence its discretized version is simply the identity matrix, as is $M_{R_p}^{-1}$.

A.2.2 Slit Reference

For the slit reference R_s , $\mathcal{L}_{R_s}^n$ is shown in Section 4.1 of [GSF07] to be $\frac{\partial}{\partial y}$, i.e., vertical first-order differential operator, which can be approximated by $M_{R_s}^{-1} = I \otimes D_n$ (see Eq. (2.19)), as $(I \otimes D_n) \text{vec}(R_s) = \text{vec}(D_n R_s I)$. Here D_n is the first-order difference matrix that performs finite differencing vertically.

A.2.3 Block Reference

For the block reference R_b , $\mathcal{L}_{R_b}^n$ is shown in Section 4.3 of [GSF07] to be $\frac{\partial^2}{\partial x \partial y}$, which can be approximated by $M_{R_b}^{-1} = D_n \otimes D_n$ (see Eq. (2.23)), as $(D_n \otimes D_n) \text{vec}(R_b) = \text{vec}(D_n R_b D_n^T)$.

Overall, the referenced deconvolution method can be easily applied to any arbitrary reference R . In contrast, the HERALDO procedure can only be applied when \mathcal{L}_R^n exists and can be constructed, which has to date only been demonstrated for special references with simple geometric shapes—so that the specific construction of \mathcal{L}_R^n is straightforward. However, it may not be easily applicable to reference choices such as the annulus [GO18] or uniformly redundant array [MBS⁺08].

⁵It is also possible that this correspondence can be extended to a larger class of reference choices. Indeed, it is easily seen that $M_R^{-1} \text{flip}(\text{vec}(\bar{R})) = e_1$, whereby M_R^{-1} plays the same role as does \mathcal{L}_R^n in Eq. (A.5).

B Proof of Theorem 3.10

Let $\eta \doteq \left\| \tilde{X} - X \right\|_F^2$. We are interested to control $|\eta - \mathbb{E}\eta|$. By similar manipulation as in Lemma 3.3, we have

$$\begin{aligned} & \left\| \tilde{X} - X \right\|_F^2 - \mathbb{E} \left\| \tilde{X} - X \right\|_F^2 \\ &= \left\langle T_R^* T_R, \left[\text{vec}(\tilde{Y}) - \text{vec}(Y) \right] \left[\text{vec}(\tilde{Y}) - \text{vec}(Y) \right]^* - \mathbb{E} \left[\text{vec}(\tilde{Y}) - \text{vec}(Y) \right] \left[\text{vec}(\tilde{Y}) - \text{vec}(Y) \right]^* \right\rangle. \end{aligned}$$

Since entries in $\text{vec}(\tilde{Y}) - \text{vec}(Y)$ have sub-exponential tails, we need Hanson-Wright type inequalities for sub-exponential random variables.

Theorem B.1 (Proposition 1.1 of [GSS19]). *Let $A \in \mathbb{R}^{n \times n}$ be a symmetric matrix and let Z_1, \dots, Z_n be a set of independent random variables with $\mathbb{E}Z_i = 0$ and $\|Z_i\|_{\psi_1} \leq M$ for all i (here $\|\cdot\|_{\psi_1}$ is the sub-exponential norm as defined in, e.g., Definition 2.7.5. of [Ver18]). Write $Z \doteq [Z_1; \dots; Z_n]$. For any $t > 0$,*

$$\mathbb{P} \left[|Z^\top A Z - \mathbb{E}Z^\top A Z| \geq t \right] \leq 2 \exp \left(-c \min \left\{ \frac{t^2}{M^4 \|A\|_F^2}, \frac{t^{1/2}}{M \|A\|^{1/2}} \right\} \right). \quad (\text{B.1})$$

Note that

$$\left\langle T_R^* T_R, \left[\text{vec}(\tilde{Y}) - \text{vec}(Y) \right] \left[\text{vec}(\tilde{Y}) - \text{vec}(Y) \right]^* \right\rangle = \left[\text{vec}(\tilde{Y}) - \text{vec}(Y) \right]^* (T_R^* T_R) \left[\text{vec}(\tilde{Y}) - \text{vec}(Y) \right].$$

So, in our problem, the random vector Z is $\text{vec}(\tilde{Y}) - \text{vec}(Y)$

$$Z_k \doteq \tilde{Y}_{ij} - Y_{ij}. \quad (\text{B.2})$$

By our Poisson model,

$$\mathbb{E} \left[\tilde{Y}_{ij} - Y_{ij} \right] = Y_{ij} - Y_{ij} = 0. \quad (\text{B.3})$$

Now we need to estimate the sub-exponential norm of a centered Poisson random variable.

Lemma B.2. *Let $Z \sim \text{Pois}(\lambda)$. We have*

$$\|Z - \lambda\|_{\psi_1} \leq C \left(\sqrt{3\lambda} + 2 \right), \quad (\text{B.4})$$

where $C > 0$ is a universal constant.

Proof. Applying the Cramer-Chernoff method to $Z - \lambda$, we obtain that (see, e.g., Page 23 of [BLM13])

$$\mathbb{P} [Z - \lambda > t] \leq \exp \{ -\lambda h(t/\lambda) \} \quad \forall t \geq 0, \quad (\text{B.5})$$

$$\mathbb{P} [Z - \lambda < -t] \leq \exp \{ -\lambda h(-t/\lambda) \} \quad \forall t \in [0, \lambda], \quad (\text{B.6})$$

where $h(u) \doteq (1+u) \log(1+u) - u$. Using that $h(u) \geq \frac{u^2}{2(1+u/3)}$, we can write the above results collectively as

$$\mathbb{P} [|Z - \lambda| > t] \leq 2 \exp \left(-\frac{t^2}{2\lambda + 2t/3} \right) \quad \forall t > 0. \quad (\text{B.7})$$

Now we will estimate the sub-exponential norm by upper bounding the moments $\mathbb{E}|Z - \lambda|^p$. We have

$$\mathbb{E}|Z - \lambda|^p = \int_0^\infty \mathbb{P} [|Z - \lambda|^p \geq u] du \quad (\text{B.8})$$

$$= \int_0^\infty \mathbb{P}[|Z - \lambda| \geq t] p t^{p-1} dt \quad (\text{B.9})$$

$$\leq 2p \int_0^\infty \exp\left(-\frac{t^2}{2\lambda + 2t/3}\right) t^{p-1} dt \quad (\text{B.10})$$

$$= 2p \int_0^{\frac{3}{2}\lambda} \exp\left(-\frac{t^2}{2\lambda + 2t/3}\right) t^{p-1} dt + 2p \int_{\frac{3}{2}\lambda}^\infty \exp\left(-\frac{t^2}{2\lambda + 2t/3}\right) t^{p-1} dt \quad (\text{B.11})$$

$$\leq 2p \int_0^{\frac{3}{2}\lambda} \exp\left(-\frac{t^2}{3\lambda}\right) t^{p-1} dt + 2p \int_{\frac{3}{2}\lambda}^\infty \exp\left(-\frac{t}{2}\right) t^{p-1} dt \quad (\text{B.12})$$

$$\leq 2p \int_0^\infty \exp\left(-\frac{t^2}{3\lambda}\right) t^{p-1} dt + 2p \int_0^\infty \exp\left(-\frac{t}{2}\right) t^{p-1} dt \quad (\text{B.13})$$

$$\leq (3\lambda)^{p/2} p \Gamma(p/2) + 2^{p+1} p \Gamma(p) \leq (3\lambda)^{p/2} p (p/2)^{p/2} + 2^{p+1} p^{p+1}, \quad (\text{B.14})$$

where we used $\Gamma(x) \leq x^x$ to obtain the very last bound. Thus,

$$\|Z - \lambda\|_{L_p} = (\mathbb{E}|Z - \lambda|^p)^{1/p} \leq 5 \left(\sqrt{3\lambda} + 2\right) p. \quad (\text{B.15})$$

We obtain the claimed result by connecting the above moment bound with the definition of sub-exponential norm, see, e.g., Proposition 2.7.1 of [Ver18]. \blacksquare

We are ready now to state the concentration of the empirical (squared) error around the expectation.

Theorem B.3. *For any of the three special (i.e., pinhole, slit, block) references, the following holds: for all $t > 0$,*

$$\mathbb{P}\left[\left|\|\tilde{X} - X\|_F^2 - \mathbb{E}\|\tilde{X} - X\|_F^2\right| \geq t\right] \leq 2 \exp\left(-c \min\left\{\frac{N_p m t^{1/2}}{\sqrt{3N_p} \|Y\|_1 \|Y\|_\infty + 2 \|Y\|_1}, \frac{N_p^4 m^4 t^2}{n^2 (\sqrt{3N_p} \|Y\|_1 \|Y\|_\infty + 2 \|Y\|_1)^4}\right\}\right). \quad (\text{B.16})$$

Here $c > 0$ is a universal constant.

Proof. By our Poisson noise model and Lemma B.2,

$$\|Y_{ij} - \tilde{Y}_{ij}\|_{\psi_1} \leq C \frac{\|Y\|_1}{N_p} \left(\sqrt{\frac{3N_p}{\|Y\|_1}} Y_{ij} + 2\right). \quad (\text{B.17})$$

So in applying Theorem B.1, we can take $M = C \frac{\|Y\|_1}{N_p} \left(\sqrt{\frac{3N_p}{\|Y\|_1}} \|Y\|_\infty + 2\right)$.

Now we estimate $\|T_R^* T_R\| = \|T_R\|^2$, and $\|T_R^* T_R\|_F$. Note the fact that for any two matrices A, B , $\|A \otimes B\| = \|A\| \|B\|$, $\|A \otimes B\|_F = \|A\|_F \|B\|_F$, and $\|AB\|_F \leq \|A\| \|B\|_F$. First, we have the following estimates

$$\|(P_2 F_{RA}^*) \otimes (P_1 F_{LA}^*)\| = \|P_2 F_{RA}^*\| \|P_1 F_{LA}^*\| = \sqrt{m} \times \sqrt{m} = m, \quad (\text{B.18})$$

and

$$\begin{aligned} \|[(P_2 F_{RA}^*) \otimes (P_1 F_{LA}^*)]^* [(P_2 F_{RA}^*) \otimes (P_1 F_{LA}^*)]\|_F &= \|[(P_2 F_{RA}^*) \otimes (P_1 F_{LA}^*)] [(P_2 F_{RA}^*) \otimes (P_1 F_{LA}^*)]^*\|_F \\ &= \|[(P_2 F_{RA}^*) \otimes (P_1 F_{LA}^*)] [(F_{RA} P_2^*) \otimes (F_{LA} P_1^*)]\|_F \\ &= \|(P_2 F_{RA}^* F_{RA} P_2^*) \otimes (P_1 F_{LA}^* F_{LA} P_1^*)\|_F \\ &= m^2 \|P_2 P_2^*\|_F \|P_1 P_1^*\|_F = m^2 n. \end{aligned} \quad (\text{B.19})$$

So specializing to the references, we have

- For the pinhole reference,

$$\|T_{R_p}\| = \frac{1}{m^2} \|(P_2 F_{RA}^*) \otimes (P_1 F_{LA}^*)\| = \frac{1}{m}, \quad (\text{B.20})$$

$$\|T_{R_p}^* T_{R_p}\|_F \leq \frac{1}{m^4} \|[(P_2 F_{RA}^*) \otimes (P_1 F_{LA}^*)]^* [(P_2 F_{RA}^*) \otimes (P_1 F_{LA}^*)]\|_F = \frac{m^2 n}{m^4} = \frac{n}{m^2}. \quad (\text{B.21})$$

- For the slit reference,

$$\|T_{R_s}\| \leq \frac{1}{m^2} \|D_n\| \|(P_2 F_{RA}^*) \otimes (P_1 F_{LA}^*)\| \leq \frac{2}{m}, \quad (\text{B.22})$$

where we used $\|D_n\| \leq 2$. Moreover,

$$\|T_{R_s}^* T_{R_s}\|_F \leq \frac{1}{m^4} \|D_n\|^4 \|[(P_2 F_{RA}^*) \otimes (P_1 F_{LA}^*)]^* [(P_2 F_{RA}^*) \otimes (P_1 F_{LA}^*)]\|_F \leq \frac{4n}{m^2}. \quad (\text{B.23})$$

- For the block reference,

$$\|T_{R_b}\| \leq \frac{1}{m^2} \|D_n\|^2 \|(P_2 F_{RA}^*) \otimes (P_1 F_{LA}^*)\| \leq \frac{4}{m}, \quad (\text{B.24})$$

$$\|T_{R_b}^* T_{R_b}\|_F \leq \frac{1}{m^4} \|D_n\|^4 \|[(P_2 F_{RA}^*) \otimes (P_1 F_{LA}^*)]^* [(P_2 F_{RA}^*) \otimes (P_1 F_{LA}^*)]\|_F \leq \frac{16n}{m^2}. \quad (\text{B.25})$$

So for all the three references, we have

$$\|T_R^* T_R\| \leq \frac{16}{m^2}, \quad \|T_R^* T_R\|_F \leq \frac{16n}{m^2}. \quad (\text{B.26})$$

Substituting the estimates into [Theorem B.1](#), we obtain the claimed result. ■

References

- [BBE17] Tamir Bendory, Robert Beinert, and Yonina C. Eldar, *Fourier phase retrieval: Uniqueness and algorithms*, Springer International Publishing, Cham, 2017.
- [BDP⁺07] Oliver Bunk, Ana Diaz, Franz Pfeiffer, Christian David, Bernd Schmitt, Dillip K Satapathy, and J Friso van der Veen, *Diffractive imaging for periodic samples: retrieving one-dimensional concentration profiles across microfluidic channels*, *Acta Crystallographica Section A* **63** (2007), no. 4, 306–314.
- [BLM13] Stéphane Boucheron, Gábor Lugosi, and Pascal Massart, *Concentration inequalities: A nonasymptotic theory of independence*, Oxford university press, 2013.
- [BPC⁺11] Stephen Boyd, Neal Parikh, Eric Chu, Borja Peleato, and Jonathan Eckstein, *Distributed optimization and statistical learning via the alternating direction method of multipliers*, *Found. Trends Mach. Learn.* **3** (2011), no. 1, 1–122.
- [BS17] David Barmherzig and Ju Sun, *A Local Analysis of Block Coordinate Descent for Gaussian Phase Retrieval*, 10th NIPS Workshop on Optimization for Machine Learning **abs/1712.0** (2017).
- [BSC⁺19] David A. Barmherzig, Ju Sun, Emmanuel J. Candès, T. J. Lane, and Po-Nan Li, *Dual-Reference Design for Holographic Coherent Diffraction Imaging*, arXiv e-prints (2019), arXiv:1902.02492.
- [BSLL18] David Barmherzig, Ju Sun, Po-Nan Li, and T J Lane, *On Block-Reference Coherent Diffraction Imaging*, *Imaging and Applied Optics 2018* (3D, AO, AIO, COSI, DH, IS, LACSEA, LS&C, MATH, pcAOP), Optical Society of America, 2018, p. CTH1B.1.

- [BTN01] A. Ben-Tal and A. Nemirovski, *Lectures on modern convex optimization*, Society for Industrial and Applied Mathematics, 2001.
- [CBB⁺06] Henry N Chapman, Anton Barty, Michael J Bogan, Sébastien Boutet, Matthias Frank, Stefan P Hau-Riege, Stefano Marchesini, Bruce W Woods, Sasa Bajt, W Henry Benner, Richard A London, Elke Plönjes, Marion Kuhlmann, Rolf Treusch, Stefan Düsterer, Thomas Tschentscher, Jochen R Schneider, Eberhard Spiller, Thomas Möller, Christoph Bostedt, Matthias Hoener, David A Shapiro, Keith O Hodgson, David van der Spoel, Florian Burmeister, Magnus Bergh, Carl Caleman, Gösta Huldt, M Marvin Seibert, Filipe R N C Maia, Richard W Lee, Abraham Szöke, Nicusor Timneanu, and Janos Hajdu, *Femtosecond diffractive imaging with a soft-X-ray free-electron laser*, *Nature Physics* **2** (2006), 839–843.
- [CESV15] E Candès, Y Eldar, T Strohmer, and V Voroninski, *Phase Retrieval via Matrix Completion*, *SIAM Review* **57** (2015), no. 2, 225–251.
- [CLS15a] E J Candès, X Li, and M Soltanolkotabi, *Phase retrieval via wirtinger flow: Theory and algorithms*, *IEEE Trans. Inf. Theory* **61** (2015), no. 4, 1985–2007.
- [CLS15b] Emmanuel J Candès, Xiaodong Li, and Mahdi Soltanolkotabi, *Phase retrieval from coded diffraction patterns*, *Applied and Computational Harmonic Analysis* **39** (2015), no. 2, 277–299.
- [DF87] J C Dainty and J R Fienup, *Phase retrieval and image reconstruction for astronomy*, *Image Recovery: Theory and Application* (H. Stark, ed.), Academic Press, 1987.
- [Els03] Veit Elser, *Phase retrieval by iterated projections*, *J. Opt. Soc. Am. A* **20** (2003), no. 1, 40–55.
- [ELS⁺04] S Eisebitt, J Löffing, W F Schlotter, M Löffler, O Hellwig, W Eberhardt, and J Stöhr, *Lensless imaging of magnetic nanostructures by X-ray spectro-holography*, *Nature* **432** (2004), 885–888.
- [ERT07] V Elser, I Rankenburg, and P Thibault, *Searching with iterated maps*, *Proceedings of the National Academy of Sciences* **104** (2007), no. 2, 418–423.
- [Fie78] J R Fienup, *Reconstruction of an object from the modulus of its Fourier transform*, *Opt. Lett.* **3** (1978), no. 1, 27–29.
- [Gab48] D Gabor, *A New Microscopic Principle*, *Nature* **161** (1948), 777–778.
- [GKL⁺08] Eric Ghigo, Jürgen Kartenbeck, Pham Lien, Lucas Pelkmans, Christian Capo, Jean-Louis Mege, and Didier Raoult, *Ameobal Pathogen Mimivirus Infects Macrophages through Phagocytosis*, *PLOS Pathogens* **4** (2008), no. 6, 1–17.
- [GO18] Tais Gorkhover and Others, *Femtosecond X-ray Fourier holography imaging of free-flying nanoparticles*, *Nature Photonics* **12** (2018), no. 3, 150–153.
- [Goo17] Joseph W. Goodman, *Introduction to fourier optics*, 4th ed., Macmillan Learning, New York, NY, USA, 2017.
- [GSF07] Manuel Guizar-Sicairos and James R Fienup, *Holography with extended reference by autocorrelation linear differential operation*, *Opt. Express* **15** (2007), no. 26, 17592–17612.
- [GSF08] ———, *Direct image reconstruction from a Fourier intensity pattern using HERALDO*, *Opt. Lett.* **33** (2008), no. 22, 2668–2670.
- [GSS19] Friedrich Götze, Holger Sambale, and Arthur Sinulis, *Concentration inequalities for polynomials in α -sub-exponential random variables*, arXiv:1903.05964 (2019).

- [Hay82] M Hayes, *The reconstruction of a multidimensional sequence from the phase or magnitude of its Fourier transform*, IEEE Transactions on Acoustics, Speech, and Signal Processing **30** (1982), no. 2, 140–154.
- [HSC15] Kuan He, Manoj Kumar Sharma, and Oliver Cossairt, *High dynamic range coherent imaging using compressed sensing*, Opt. Express **23** (2015), no. 24, 30904–30916.
- [Jag16] Kishore Jaganathan, *Convex programming-based phase retrieval: Theory and applications*, 2016.
- [JEH15] K. Jaganathan, Y. Eldar, and B. Hassibi, *Phase retrieval with masks using convex optimization*, 2015 IEEE International Symposium on Information Theory (ISIT), June 2015, pp. 1655–1659.
- [JEH16] Kishore Jaganathan, Yonina C. Eldar, and Babak Hassibi, *Phase retrieval: an overview of recent developments*, 263–296.
- [JJB⁺08] I. Johnson, K. Jefimovs, O. Bunk, C. David, M. Dierolf, J. Gray, D. Renker, and F. Pfeiffer, *Coherent diffractive imaging using phase front modifications*, Phys. Rev. Lett. **100** (2008), 155503.
- [KAKK72] S Kikuta, S Aoki, S Kosaki, and K Kohra, *X-ray holography of lensless Fourier-transform type*, Optics Communications **5** (1972), no. 2, 86–89.
- [KH90] Wooshik Kim and Monson H. Hayes, *Phase retrieval using two fourier-transform intensities*, J. Opt. Soc. Am. A **7** (1990), no. 3, 441–449.
- [LCL⁺08] Y. J. Liu, B. Chen, E. R. Li, J. Y. Wang, A. Marcelli, S. W. Wilkins, H. Ming, Y. C. Tian, K. A. Nugent, P. P. Zhu, and Z. Y. Wu, *Phase retrieval in x-ray imaging based on using structured illumination*, Phys. Rev. A **78** (2008), 023817.
- [LHM⁺12] N D Loh, C Y Hampton, A V Martin, D Starodub, R G Sierra, A Barty, A Aquila, J Schulz, L Lomb, J Steinbrener, R L Shoeman, S Kassemeyer, C Bostedt, J Bozek, S W Epp, B Erk, R Hartmann, D Rolles, A Rudenko, B Rudek, L Foucar, N Kimmel, G Weidenspointner, G Hauser, P Holl, E Pedersoli, M Liang, M S Hunter, L Gumprecht, N Coppola, C Wunderer, H Graafsma, F R N C Maia, T Ekeberg, M Hantke, H Fleckenstein, H Hirsemann, K Nass, T A White, H J Tobias, G R Farquar, W H Benner, S P Hau-Riege, C Reich, A Hartmann, H Soltau, S Marchesini, S Bajt, M Barthelmess, P Bucksbaum, K O Hodgson, L Strüder, J Ullrich, M Frank, I Schlichting, H N Chapman, and M J Bogan, *Fractal morphology, imaging and mass spectrometry of single aerosol particles in flight*, Nature **486** (2012), 513–517.
- [LU62] Emmett N Leith and Juris Upatnieks, *Reconstructed wavefronts and communication theory*, Journal of the Optical Society of America **52** (1962), no. 10, 1123–1130.
- [Luk05] D Russell Luke, *Relaxed averaged alternating reflections for diffraction imaging*, Inverse Problems **21** (2005), no. 1, 37–50.
- [LZGJ⁺18] Yuan Hung Lo, Lingrong Zhao, Marcus Gallagher-Jones, Arjun Rana, Jared J. Lodico, Weikun Xiao, B C Regan, and Jianwei Miao, *In situ coherent diffractive imaging*, Nature Communications **9** (2018), no. 1, 1826.
- [MA08] A V Martin and L J Allen, *Direct retrieval of a complex wave from its diffraction pattern*, Optics Communications **281** (2008), no. 20, 5114–5121.
- [Mar07] Stefano Marchesini, *Invited article: A unified evaluation of iterative projection algorithms for phase retrieval*, Review of scientific instruments **78** (2007), no. 1, 11301.
- [MBS⁺08] Stefano Marchesini, Sébastien Boutet, Anne E. Sakdinawat, Michael J. Bogan, SÇÖa Bajt, Anton Barty, Henry N. Chapman, Matthias Frank, Stefan P. Hau-Riege, Abraham Szöke, Congwu Cui, David A. Shapiro, Malcolm R. Howells, John Spence, Joshua W. Shaevitz, Joanna Y. Lee, Janos Hajdu, and Marvin M. Seibert, *Massively parallel x-ray holography*, Nature Photonics **2** (2008), no. 9, 560–563.

- [MCKS99] Jianwei Miao, Pambos Charalambous, Janos Kirz, and David Sayre, *Extending the methodology of X-ray crystallography to allow imaging of micrometre-sized non-crystalline specimens*, *Nature* **400** (1999), 342–344.
- [Mil90] R P Millane, *Phase retrieval in crystallography and optics*, *J. Opt. Soc. Am. A* **7** (1990), no. 3, 394–411.
- [MIRM15] Jianwei Miao, Tetsuya Ishikawa, Ian K. Robinson, and Margaret M. Murnane, *Beyond crystallography: Diffractive imaging using coherent x-ray light sources*, *Science* **348** (2015), no. 6234, 530–535.
- [OS09] Alan V. Oppenheim and Ronald W. Schaffer, *Discrete-time signal processing*, 3rd ed., Prentice Hall Press, Upper Saddle River, NJ, USA, 2009.
- [PPP07] S G Podorov, K M Pavlov, and D M Paganin, *A non-iterative reconstruction method for direct and unambiguous coherent diffractive imaging*, *Opt. Express* **15** (2007), no. 16, 9954–9962.
- [RVW⁺01] I K Robinson, I A Vartanyants, G J Williams, M A Pfeifer, and J A Pitney, *Reconstruction of the Shapes of Gold Nanocrystals Using Coherent X-Ray Diffraction*, *Phys. Rev. Lett.* **87** (2001), no. 19, 195505.
- [SC91] H. Sahinoglou and S. D. Cabrera, *On phase retrieval of finite-length sequences using the initial time sample*, *IEEE Transactions on Circuits and Systems* **38** (1991), no. 8, 954–958.
- [Sch18] W Schottky, *Über spontane Stromschwankungen in verschiedenen Elektrizitätsleitern*, *Annalen der Physik* **362** (1918), no. 23, 541–567.
- [SEC⁺15] Yoav Shechtman, Yonina C Eldar, Oren Cohen, Henry Nicholas Chapman, Jianwei Miao, and Mordechai Segev, *Phase retrieval with application to optical imaging: a contemporary overview*, *IEEE signal processing magazine* **32** (2015), no. 3, 87–109.
- [SLLF12] M Saliba, T Latychevskaia, J Longchamp, and H Fink, *Fourier Transform Holography: A Lensless Non-Destructive Imaging Technique*, *Microscopy and Microanalysis* **18** (2012), no. S2, 564–565.
- [Str16] Gilbert Strang, *Introduction to Linear Algebra, Fifth Edition*, Wellesley-Cambridge Press, 2016.
- [The10] The Center for X-ray Optics, Lawrence Berkeley National Laboratory, *X-ray transmission of solids*, 2010.
- [TreND] W Trench, *Inverses of lower triangular toeplitz matrices*, N.D., unpublished.
- [Ver18] Roman Vershynin, *High-dimensional probability: An introduction with applications in data science*, Cambridge University Press, September 2018.
- [Wal63] Adriaan Walther, *The question of phase retrieval in optics*, *Optica Acta: International Journal of Optics* **10** (1963), no. 1, 41–49.
- [WTT⁺16] I S Wahyutama, G K Tadesse, A Tünnermann, J Limpert, and J Rothhardt, *Influence of detector noise in holographic imaging with limited photon flux*, *Opt. Express* **24** (2016), no. 19, 22013–22027.
- [WYLM12] Zaiwen Wen, Chao Yang, Xin Liu, and Stefano Marchesini, *Alternating direction methods for classical and ptychographic phase retrieval*, *Inverse Problems* **28** (2012), no. 11, 115010.
- [XMR⁺14] Gang Xiong, Oussama Moutanabbir, Manfred Reiche, Ross Harder, and Ian Robinson, *Coherent X-Ray Diffraction Imaging and Characterization of Strain in Silicon-on-Insulator Nanostructures*, *Advanced Materials* **26** (2014), no. 46, 7747–7763.
- [ZO10] Diling Zhu and Others, *High-resolution X-ray lensless imaging by differential holographic encoding*, *Physical review letters* **105** (2010), no. 4, 43901.